Brodogradnja Volume 77 Number 4 (2026) 77408

University of Zagreb
Faculty of Mechanical
Engineering and Naval
Architecture

journal homepage: www.brodogradnja.fsb.hr

Brodogradnja

An International Journal of Naval Architecture and
Ocean Engineering for Research and Development

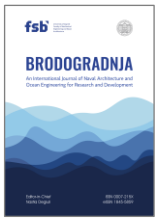

Low-frequency structural vibration reduction in stiffened panels using integrated acoustic black holes

Giovanni Rognoni[1,*], *Emanuele Brocco*[2], *Giada Kyaw Oo D'Amore*[1], *Marco Biot*[1]

[1]*Department of Engineering and Architecture, University of Trieste, Via Alfonso Valerio 7/4, Trieste, 34127, Italy*
[2]*C.S.N.I: Scarl, Corso Perrone 27/R, Genova, 16152, Italy*

ARTICLE INFO

Keywords:
Marine Structures
Waveguide
Structural Intensity
Metamaterial
Mock-up

ABSTRACT

Stiffened panels are the fundamental elements of ship hulls, composing main structures, such as decks and bulkheads. Due to their key role in hull dynamics, especially in the range of machinery-induced vibrations propagating throughout the structure, reducing their mobility is expected to contribute to an overall decrease in the vessel's acoustic footprint. An emerging technology with high potential for reducing structural vibrations is the Acoustic Black Hole. When integrated into the ship hull, these devices act as energy wells for flexural waves. Over the past two decades, Acoustic Black Holes have been extensively investigated through analytical, numerical, and laboratory-scale experiments. Yet, their practical integration into ship-representative structures remains unexplored. In this paper, two Acoustic Black Holes were integrated into the plating of a mock-up representative of a typical ship stiffened panel. Their placement was defined based on the structural intensity approach; an experimental campaign was conducted to demonstrate the vibration mitigation effect obtained. The results show the suppression of targeted modes and the reduction of vibrational velocity obtained on the stiffened panel plating. This research aims to be the first step towards implementing this technology onboard ships, paving the way for its future application in full-scale marine structures.

1. Introduction

1.1 Vibration propagation on ships

Ship vibrations have been an issue for naval architects since the advent of mechanical propulsion. Early testimonies of passengers' complaints can be found in century-old documents [1, 2] and discussions on how to reduce them were already in place [3]. One hundred years later, methods and tools have improved; however, the study of how vibrations propagate from sources to the hull and superstructures is still an object of research [4-6]. For large commercial ships, propellers and onboard machinery generate structural vibrations above the global modes' frequencies (over 2 to 5 Hz). Pressure-induced vibrations from propellers [7] propagate to the hull, generating discomfort [8]. Equally, vibrations due to onboard machinery such as engines, generators,

* Corresponding author.
E-mail address: giovanni.rognoni@dia.units.it

https://doi.org/10.21278/brod77408
Received 28 January 2026; Received in revised form 12 May 2026; Accepted 15 May 2026
Available online 1 June 2026
ISSN 0007-215X; eISSN 1845-5859

gearboxes, hydraulic systems, pumps, and compressors are transmitted to the foundations and propagate across the hull [9].

Ship structures are made by an assembly of beams, girders, stiffeners, and plating. The hull dynamic can be described on three vibration levels [10, 11]: hull girder, main structures (grillages of decks and bulkheads) and local structures. Figure 1 shows the three levels. Hull girder analysis is performed to identify the ship's global modes and those modes involving the superstructures [12, 13]. The second level regards the global modes of the main structures, large structures made by stiffened panels supported by beams and girders. They can be analysed by fine-mesh partial FE models or equivalent single-layer theory [14]. In main structures, the energy is transported by flexural waves having a wavelength greater than the stiffened panels' main dimensions. Local structures must be analysed using "ad hoc" methods, considering the interaction between stiffeners and plating. Clarkson et al. [15] showed that adjacent panels across a frame vibrate independently of one another, as the frames act like rigid boundaries. These observations led researchers to formulate a theory of propagation based on a waveguide approach [16, 17]. This theory, suggested by the experimental evidence at the time, assumed that the rigid structures are fixed boundaries and that the energy propagates mainly through flexural waves in the plating. The hypothesis, however, does not explain why applying a viscoelastic material (VEM), which dissipates energy by flexural deformations, would not stop the propagation when placed at some point of the propagation path. Subsequent studies performed using finite element analysis showed that, while the flexural waves are the dominant form of energy in the stiffened-panel plating, longitudinal waves are dominant in the stiffeners [18-20].

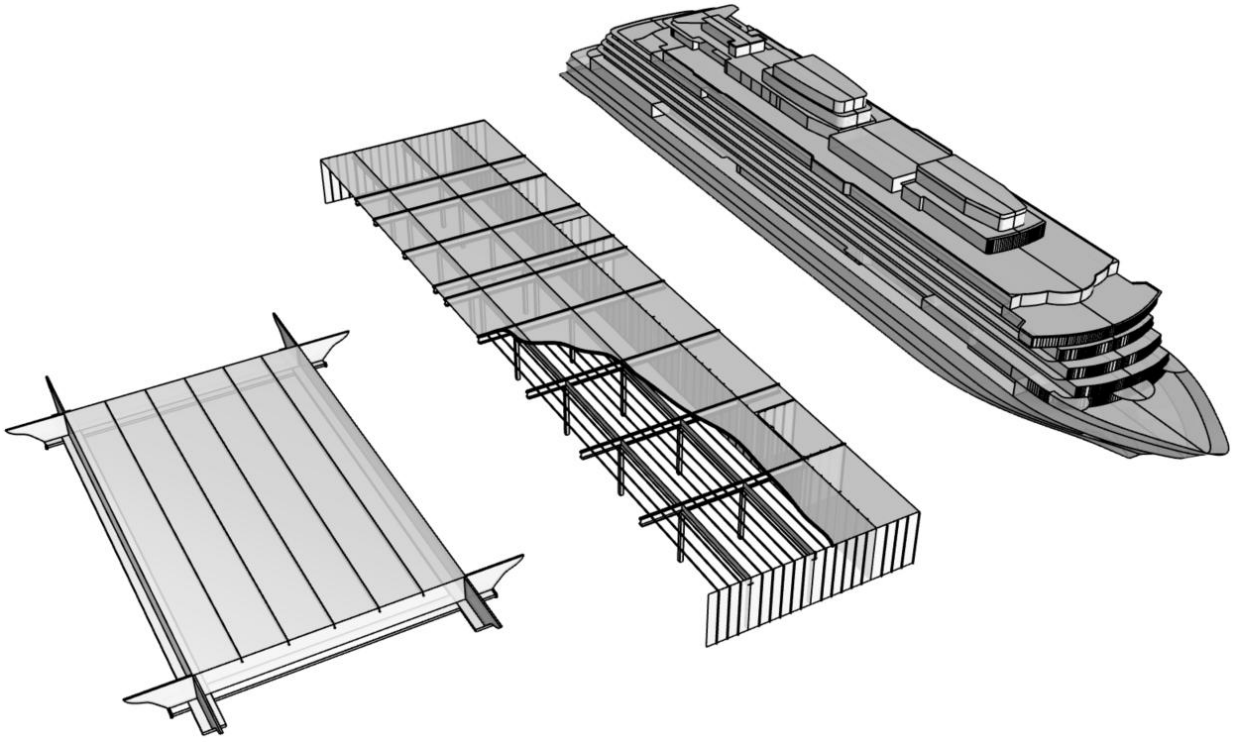

Fig. 1 Subsequent levels in ship structure dynamic analysis: hull-girder; main structure (deck between transverse bulkheads); local structure (stiffened panel between main beams and girders)

There are three possible ways to reduce structural vibrations on board: decrease the vibrations at the source, act on the transmission path between source and target, and mitigate the vibration at the target. Sources can be isolated from the hull: engines and machinery can be suspended on resilient mounts to prevent the transmission of imbalance forces to the foundations [9, 21]. Acting on the propellers is more challenging, as it would need a redesign or an isolation of the area affected by the induced pressures [22]. Disrupting the transmission of energy between source and target is not an easy task. The longitudinal waves that carry most of the energy in stiffeners should be interrupted to prevent transmission. However, this is impossible using VEMs, which work on flexural waves. On-plating application of VEM on the in-between path demonstrated to be ineffective [23, 24]. For modes of decks and bulkheads, the VEM effectiveness is limited by its relatively

low shear deformation: the constraining plate bending stiffness is too low compared to that of the main structure. An alternative would be the application of bandgap theory as suggested by Chen et al. [25] and Li et al. [26], which exploits the bandgap properties of the periodic arrangement of the stiffened panels which make up the main structures.

When sources isolations have been optimized, acting on the target is generally more effective than acting between source and target. The VEMs are effective when placed locally on the target. Alternatively, solutions such as suspended floors can be used in accommodation areas [9, 27]. However, passive isolation systems have their limits: VEMs need vast application areas and usually they require the presence of metal constraining plates; both VEMs and suspended floors are characterised by potential flammability, toxicity, and made by materials having low eco-sustainability (polymers and mineral wools); lastly, they suffer from an inherent inefficiency at low frequency.

1.2 A new solution: Acoustic Black Holes

A new potential solution for the mitigation of structural vibrations is represented by the Acoustic Black Hole (ABH). These devices operate based on a phenomenon first documented by Mironov [28]: when a flexural wave propagates through a tapered beam, its velocity decreases as it approaches the tip, ultimately tending to zero as it reaches the beam's end. This effect theoretically prevents the wave from reflecting back, making the ABH an "energy well." An ABH's ability to interact with bending waves depends on its geometry, which determines a parameter called the cut-on frequency. This frequency sets a limit above which flexural waves are trapped in the ABH. By setting the ABH cut-on frequency to very low values, increasing mass and length, it interacts with low-frequency vibrations, making it an ideal candidate for addressing machinery-originated vibrations.

Although the potential of ABH is recognised, not many practical applications can be found in scientific literature. The study of ABH was limited to analytical, numerical, and experimental tests performed on small-sized samples in a laboratory environment. Moreover, most of these studies involve Embedded ABH, indentations created inside a host structure [29-34]. This solution effectively absorbs flexural energy, but the reduction in thickness is incompatible with the structural function of beams and plates in a ship's hull. An alternative solution is to use the ABH as an external device attached to the hull. In this way, the integrity of the hull is preserved, as the thickness reduction is made on the external ABH and not on the plating.

This typology of ABH, also called Integrated ABH, was used in this paper, externally connected to the hull. The first application of ABHs as attached devices was proposed by Zhou and Cheng [35] who called it an Acoustic Black Hole - Resonant Beam Damper. They observed two dissipation effects: interaction-dominated energy absorption (tuned-damper effect) and damping-dominated energy absorption (damping enhancement). In the first case, the ABH works as a dynamic vibration absorber, and the peaks affected show the typical splitting in two additional peaks; in the second case, it works as a waveguide, enhancing the damping-dominated effect and reducing the affected peaks. In some cases, a combination of the two dissipation effects was observed. The paper by Zhou and Cheng [35] paved the way for other integrated ABH solutions. A similar application was proposed by Li et al. [36] and Wen et al. [37]. Ji et al. [38] suggested a device whose shape was circular, such that it could affect waves propagating in multiple directions. The same authors then modified the geometry, making a circular eccentric vibration absorber [39]. A different version of the circular ABH was eventually presented by Zhao et al. [40]. Lee and Jeon [41] presented a spiral ABH designed to reduce the space occupied and developed preliminary calculations to verify if it would behave similarly to a linear ABH [42]. The authors concluded that the two geometries work approximately in the same manner. The investigations on spiral ABH were carried out by Park et al. [43], who used the concept of structural intensity to identify the best position of four devices on a plate. The work on spiral ABH is still ongoing [44]. An experimental application on an automotive engine was presented by Zhang et al. [45].

Studies on the applications of ABHs on ships are limited. ABHs were mentioned by Smith and Rigby [27] in a paper on the state-of-the-art solutions and new potential technologies to reduce radiated noise by ships. The authors assigned to each analysed solution a Technology Readiness Level (TRL) measuring the maturity of the technology in the context of the marine field. State-of-the-art technologies for machinery noise

prevention were given a high TRL (7 - 9), while new alternative technologies obtained lower TRL levels. ABH were given an estimated TRL of 3 to 4.

Between 1980 and 1990, the United States Navy carried out studies on attached absorbing waveguides [46-48]. They highlighted that tapered beams improve the dissipation effect, coming to the same conclusion as Mironov. It is unknown if the US Navy studies led to practical applications of waveguides on board vessels. As for ABHs, Bowyer et al. [49] proposed the integration of an ABH termination in turbofan blades; cylindrical ABH structures were studied by Deng et al. [50], who intended this solution to be implemented in structures such as submarine hulls. Liu et al. [51] proposed a plastic panel with embedded ABH-shaped openings to be applied to the hull plating to prevent noise transmission. Kyaw Oo D'Amore et al. [52] proposed an application of honeycomb ABH-based panels for increasing comfort on board providing numerical results. In the present study we investigated the application of external ABHs on a typical ship structure for the first time, with the aim of reducing hull-plating structural vibrations.

1.3 Approach to the problem

In this paper, we decided to focus on the stiffened panel (Figure 2), considered as the base unit element of a ship hull from a vibrational point of view [53]. A reduction of the mobility on several of these sub-units would result in a decrease of the structural vibration when the dynamic is governed by the stiffened panel modes. Due to the typical plate thickness used in marine structures and the distribution of weights on board, the number of modes of stiffened panels in the low- to medium- frequency range associated with machinery and propeller-induced vibrations can be several hundred [10]. The contribution of these modes grows with frequency, and they define the hull dynamics above the frequencies of the main structure modes. To achieve vibration reduction, we used two ABHs to suppress the flexural modes of a stiffened panel, absorbing and dissipating the vibrational energy when placed in strategic locations on a structure. We decided to limit the analysis to the range between 10 and 400 Hz, where the energy due to machinery structural vibration is more difficult to mitigate with traditional solutions.

Fig. 2 Typical ship deck stiffened structure

This paper presents a first experimental implementation of ABHs on a mock-up replicating a typical ship stiffened panel. It is organised as follows: the ABH working principle, the design criterion selected, and the prototypes manufactured for the experiment are described in section 2.1; the mock-up of the stiffened panel is described in section 2.2, followed in section 2.3 by the description of the numerical FE models used in section 2.4 to determine the position of the ABH on the mock-up, based on the structural intensity approach; the experimental setup is described in section 2.5. Section 3 collects the results: a short assessment on the quantitative energy dissipated by the different FE models used is presented in section 3.1; then, the experimental results are presented and discussed: first in narrowband (3.2), then in broadband (3.3), and finally as overall cumulative values on the entire mock-up surface and on each sub-panel (3.4); conclusions close the paper in section 4.

2. Methods

2.1 ABH working principle, design, and prototypes

The ABH effect arises in a beam when the profile decreases following this particular law [28]:

$$h(x) = \varepsilon\, x^m \tag{1}$$

where x is the coordinate of a point along the length of the ABH, ε and m are two constants. Equation 1 satisfies the condition of "sufficient smoothness" which enables the ABH effect, given by:

$$\frac{\mathrm{d}\kappa(x)}{\mathrm{d}x}\frac{1}{\kappa(x)^2} \ll 1 \tag{2}$$

where κ is the bending wavenumber which depends on the working frequency ω, the beam density ρ, elastic modulus E, and thickness h(x):

$$\kappa(x)=\left(\frac{12\,\omega^2\rho}{E\,h(x)^2}\right)^{\frac{1}{4}} \tag{3}$$

When the ABH effect occurs, the bending waves travelling from the beam's constant thickness end to the reduced thickness tip do not reflect back. Mathematically, decreasing the thickness to zero generates a point of singularity where the energy is trapped. In practical applications, however, a perfect zero-thickness termination is not feasible, and most energy bounces back. To overcome this limitation, scientists naturally considered increasing the damping capacity of the ABH wedge [29, 54, 55]. Viscoelastic materials (VEM) are now accepted as a common practice to achieve the desired results, compensating for the problems due to manufacturing quasi-zero thickness terminations. Deng et al. [56] and Kim and Lee [57] highlighted that a passive-constrained layer configuration could be used to increase the damping performance.

ABHs work above a specific value called the cut-on frequency, which defines the minimum working frequency. Two authors provided two equations to estimate this frequency: the first equation was provided by Aklouche et al. [58], who analysed an ABH indentation embedded in an infinite plate, considering it a penetrable scatterer, i.e., an obstacle with an internal wave field:

$$f_{\text{cut-on}_1} = \frac{h_0}{2\pi L^2}\sqrt{\frac{E\,[n^2(n^2\text{-}30\nu\text{+}22)\text{-}24\nu\text{+}40}{12\rho(1\text{-}\nu^2)}} \tag{4}$$

This equation was obtained for a power law coefficient m equal to 2. L is the theoretical length of the ABH, and h_0 is the initial thickness of the beam or plate hosting the ABH. E, ν, and ρ are the elastic modulus, the Poisson's coefficient, and the density of the plate, respectively; n is the circumferential order of Bessel's function used to solve the governing equations of the problem.

A second equation was developed by Lee and Jeon [42], who calculated both the cut-on frequencies of a standard and a curved ABH. The equation they derived is the following:

$$f_{\text{cut-on}_1} = \frac{h_0}{2\pi}\sqrt{\frac{E}{12\rho}}h_0\left(\frac{1.94}{L}\right)^2 \tag{5}$$

The difference arises from the different approaches adopted to develop the equations. Aklouche et al. [58] used a Kirchhoff model for infinite plates, and Lee and Jeon used the Euler-Bernoulli equations for a tapered beam [59]. Although Aklouche et al. [58] formulation is based on an embedded circular ABH in a plate, it can be extended to an integrated ABH beam, considering the longitudinal section. However, the Lee and Jeon formulation seems more appropriate for external ABH beams. Using the same material,

length, and thickness, Equation (4) with $n = 0$ (fundamental bending mode) gives a cut-on frequency approximately 1.6 times higher than Equation (5), resulting in a more conservative approach.

The cut-on frequency was used as the main parameter for designing the ABH. We used Equation (4) (the most conservative) to calculate the ABH length by selecting the material and the starting and ending thicknesses. Two materials were used: steel and a polyacetal resin called Delrin (POM-C) [60]. Their mechanical characteristics are reported in Table 1. All the prototypes were made through a milling process.

Table 1 ABH materials characteristics

	Steel	Pom-C
E (MPa)	206000	2600-3000
ν (-)	0.3	0.44
ρ (kg/m^3)	7850	1420

The design was based on the steel prototypes, selecting a target cut-on frequency of 30 Hz, the exponential coefficient was $m = 2$, and the starting thickness was 20 mm, giving a total theoretical ABH length of 971 mm (without ending truncation). By selecting the ending thickness as 2 mm, the ABH net length decreases to 664 mm. A 100 mm extension to allow enough clearance for a connecting vertical bracket was added to the ABH end, making the total length of the device equal to 764 mm. The geometrical details are reported in Figure 3a. The cut-on frequency by Equation (5) is 19 Hz. The device's width was 100 mm, and a 2 mm layer of VEM was applied along its length, excluding the 100 mm extension used to weld the bracket. A 2 mm constraining plate is also applied to maximise the viscoelastic damping effect. No optimization was performed on the viscoelastic layer thickness. The focus of the paper was on the effect of the ABH on the stiffened panel rather than the absolute performance of the ABH itself. The literature indicates that the most important part to cover to enhance energy dissipation is the tip [61, 62], however, we extended it to all the ABH cause to guarantee the maximum dissipative effect.

Two versions of these ABH were made: Model 1 and Model 2. In Model 1, the connecting bracket, measuring 100 x 80 x 15 mm, is welded to the ABH; in Model 2, a 100 mm wide 100 x 10 symmetric L-section support is screwed to the ABH. Model 2 is designed to make the application more practical and to investigate the effect of a different connection between ABH and the structure. While Model 1 was only manufactured in steel, Model 2 was manufactured using steel (Model 2.1) and POM-C (Model 2.2). The polyacetal sample has a different cut-on frequency due to its characteristics. The cut-on frequency is 8.53 Hz, according to Aklouche, Equation (4), and 5.35 Hz, according to Lee, Equation (5). No additional damping coating was applied to Model 2.2. The samples manufactured are shown in Figure 3b. The three models weigh 8.65, 9.32, and 2.85 kg (the steel L-support is included).

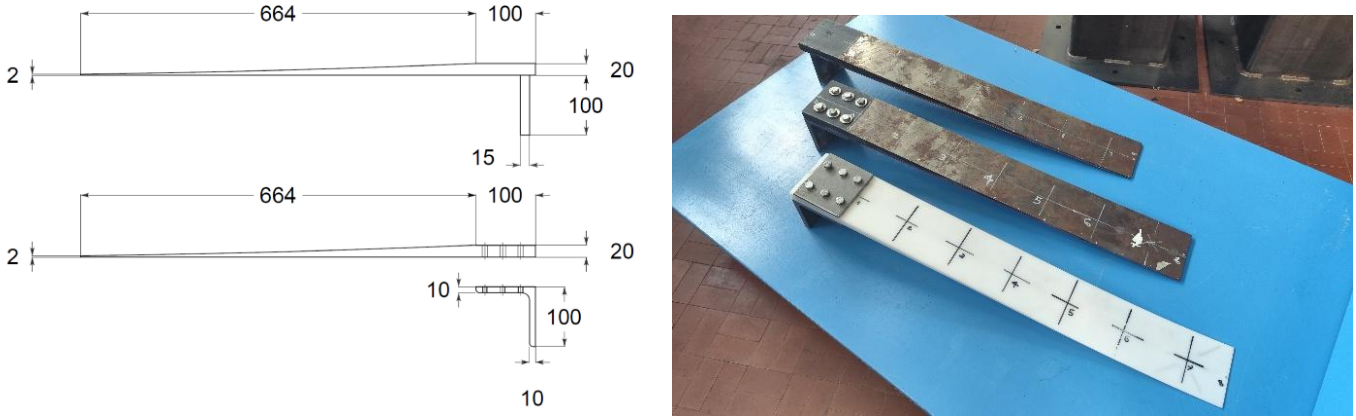

Fig. 3 a) ABH Model 1 and Model 2 technical drawings (dimensions in mm) b) ABH Model 1, Model 2.1, and Model 2.2

2.2 Stiffened panel mock-up

The mock-up used to perform the experiments represents the dynamics of a typical ship hull stiffened panel between primary structural members (Figure 4a). It is made by a 3020 mm side square steel plate having a thickness of 5 mm and reinforced by six L-section 100 x 80 x 8 mm stiffeners spaced 600 mm in the longitudinal direction and two 300 x 8 mm external beams in the transverse direction. The table is suspended on four springs at its corners, decoupling it from the sustaining pillars and simulating a condition of free oscillation (Figure 4b). The four corners rest on four 200 x 200 x 20 mm plates, reinforced by two rectangular brackets measuring 300 x 80 x 8 mm. A sketch of the structure is shown in Figure 4c which also shows the frame of reference adopted. The five sub-panels forming the plating were named P1, P2, P3, P4, and P5 as indicated.

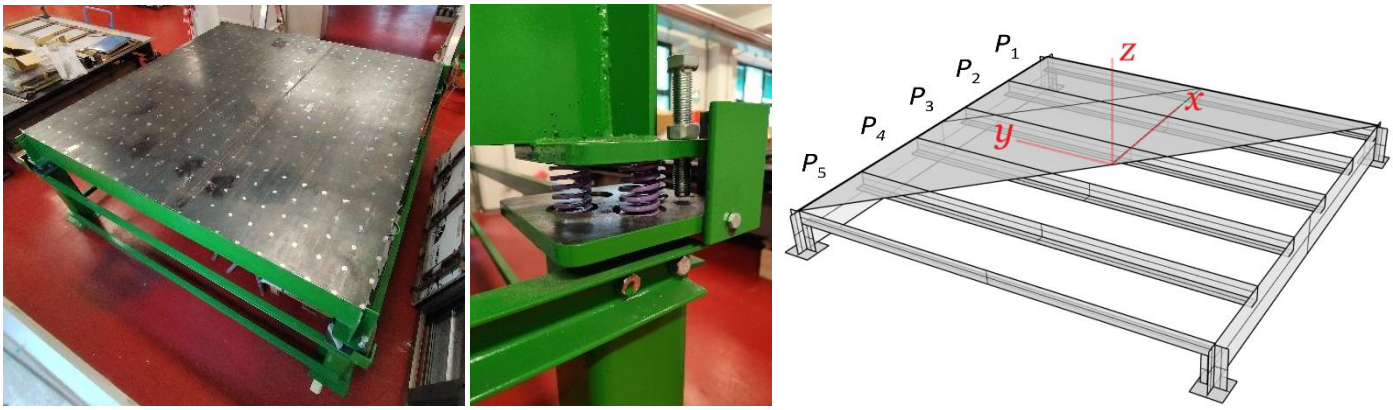

(a) (b) (c)

Fig. 4 Experimental facility: a) the mock-up at University of Trieste b) mock-up supporting spring c) graphical representation of the mock-up showing the structure, frame of reference, and the panel numbering

2.3 Numerical model

The numerical FE models of the ABHs and the mock-up were developed to calculate and analyse the vibrational energy propagation on the mock-up to position the ABHs. The two models were created using Hexagon Nastran version 2024.1. The ABH FE model, shown in Figure 5, was modelled using 8-nodes hexahedral elements. Their length varies between 1 mm on the tip and 5 mm near the supporting bracket, the width was 2 mm, and the height varies between 0.66 mm near the tip and 4 mm in the constant-thickness ending part of the ABH. The maximum elements' aspect ratio on the ABH body is below 3. The models' VEM layer and the constraining plate were discretised using three elements along the thickness. This led to a higher maximum aspect ratio (around 7) in the area far from the ending tip, where the elements' length increases.

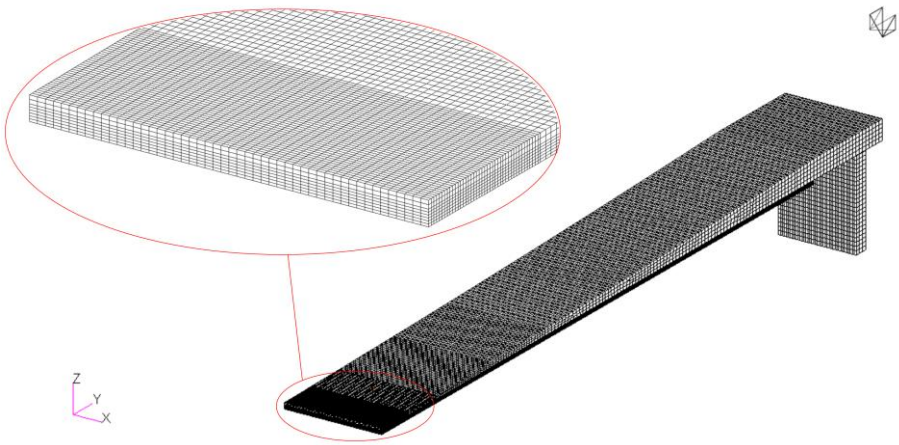

Fig. 5 FE model of the ABH

The maximum frequency that can be described using this mesh and considering ten elements per wavelength is over 3500 Hz. The FE model of the mock-up was discretised using 10 mm side square elements having shell properties (in-plane and flexural rigidity). This mesh allows for well-discretised modes having up to 7 lobes on the short sub-panel side. These modes are estimated to be over the 400 Hz limit considered in this paper. The loss factor η and the elastic modulus E of steel (Figure 6a) and VEM (Figure 6b) were estimated by experimental tests on small samples using the cantilever beam method [63]. The densities used were $\rho = 7850$ kg/m^3 for steel and 1300 kg/m^3 for the VEM. The VEM Poisson coefficient ν used is 0.4.

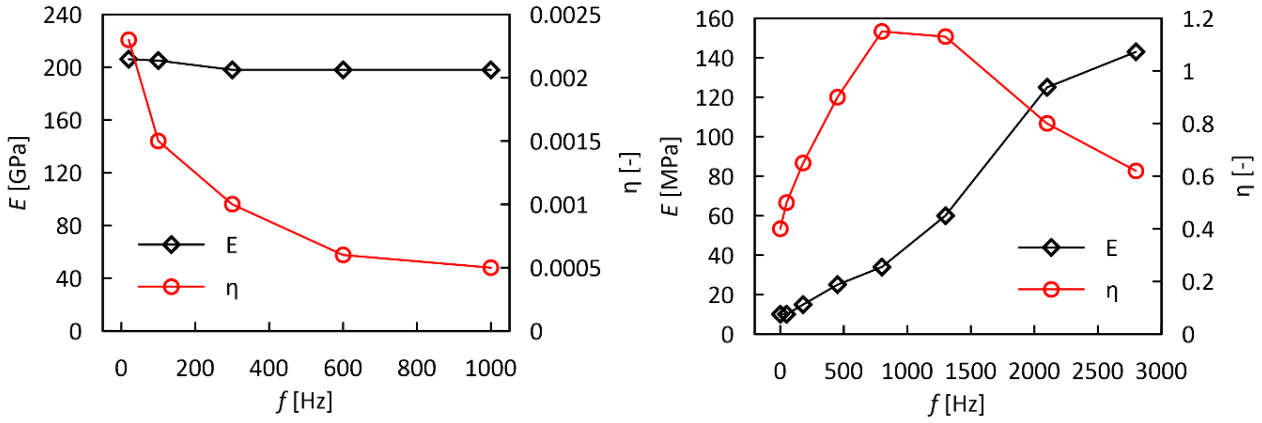

(a) (b)

Fig. 6 Elastic modulus and loss factor values used in the FE model: a) steel b) viscoelastic material

2.4 ABH positioning

The position of an ABH is crucial for its effectiveness on the host structure. ABHs are mode selective, which means that, depending on their location on the host structure, they affect specific vibration modes. Park et al. [43] used structural intensity (SI) to locate four prototypal spiral ABHs in different positions and with different orientations on a rectangular steel plate. This approach followed similar studies performed by other authors to place patches of constrained layer damping material to reduce the surface vibration of a plate [64, 65]. SI is defined as the vibrational power flow per unit cross-sectional area for a dynamically loaded plate or beam [66]. SI, introduced by Pavić [67], is calculated as follows:

$$\vec{I} = -\hat{\sigma}(t) \cdot \vec{v}(t) \tag{6}$$

where $\hat{\sigma}$ and $\vec{v}$ are the stress tensor and the velocity vector at a point of the structure. The structural intensity $\vec{I}$ is related to the energy W flowing through a section of area A for a time T by the following equation:

$$W = \int_A \int_0^T \vec{I}(t) \cdot \vec{n}_A \mathrm{d}t \, \mathrm{d}A \tag{7}$$

where $\vec{n}$ is the normal vector to the cross-sectional area A. The underlying idea of using SI to position a dissipating device is to intercept the energy flow and redirect it to these devices, where energy will be dissipated (working principle of waveguides). SI is calculated numerically [68] using typical FE software variables. For a frequency ω, the SI for a plate element can be expressed by:

$$I_x(\omega) = -\frac{1}{2}\left(N_x \dot{u}^* + N_{xy}\dot{v}^* + Q_x \dot{w}^* + M_x \dot{\theta}_y{}^* - M_{xy}\dot{\theta}_x{}^*\right) \tag{8}$$

$$I_y(\omega) = -\frac{1}{2}\left(N_y \dot{v}^* + N_{yx}\dot{u}^* + Q_y \dot{w}^* - M_y \dot{\theta}_x{}^* + M_{yx}\dot{\theta}_y{}^*\right) \tag{9}$$

where u, v, w, θ_x and θ_y are the translational and angular displacements, N_x and N_y are in-plane normal forces, N_{xy} and N_{yx} are the in-plane shear forces ($N_{xy} = N_{yx}$), M_x and M_y are the bending moments, M_{xy} and M_{yx} are

the twisting moments ($M_{xy} = M_{yx}$), and Q_x and Q_y are the transverse shear forces. The notation $(\cdot)^*$ indicates the complex conjugate of $(\cdot)$.

SI is a complex quantity; its real part is called active, while its imaginary part is called reactive [69, 70]. The active SI is related to damping and energy radiation; it highlights energy flowing paths from the sources to the points of dissipation. Reactive SI relates to the difference between elastic and kinetic energies; its field typically shows the shape of the natural modes. It is debated which component is the most important when determining the location of a vibration-mitigating system on a structure. Gavrić et al. [71] suggested comparing the absolute values of active and reactive SI to decide whether the vibrations are propagative or reverberant.

Stiffened panel modes can be divided into global modes, when sub-panels and stiffeners deform together, and local modes, when the deformation of sub-panels and stiffeners is separated. Within our context, reactive SI was used to understand which modes of the stiffened panel are affected depending on the position of the ABHs. Two ABHs were placed; the position of the first one was determined by the outcome of a numerical study [72] focused on assessing its effectiveness on the mock-up central panel P3 when the force is directly exciting the sup-panel plating S_1. Since it turned out working on local sub-panel modes developing longitudinally, position S_2 was selected to be complementary to position S_1, with the objective of tackling the global modes developing transverse to the framing system and unaffected by the first ABH. The two ABH positions are defined using as a reference the origin shown in Figure 4c and measuring the distance between it and the geometrical centre of the ABH supporting bracket cross-sectional area: S_1 = (30, 820, 0) and S_2 = (550, -10, 0). The ABH in position S_1 was aligned with the y direction, while the ABH mounted in position S_2 was aligned with the x direction, as shown in Figure 7a. Figure 7b shows the two ABH welded to the mock-up.

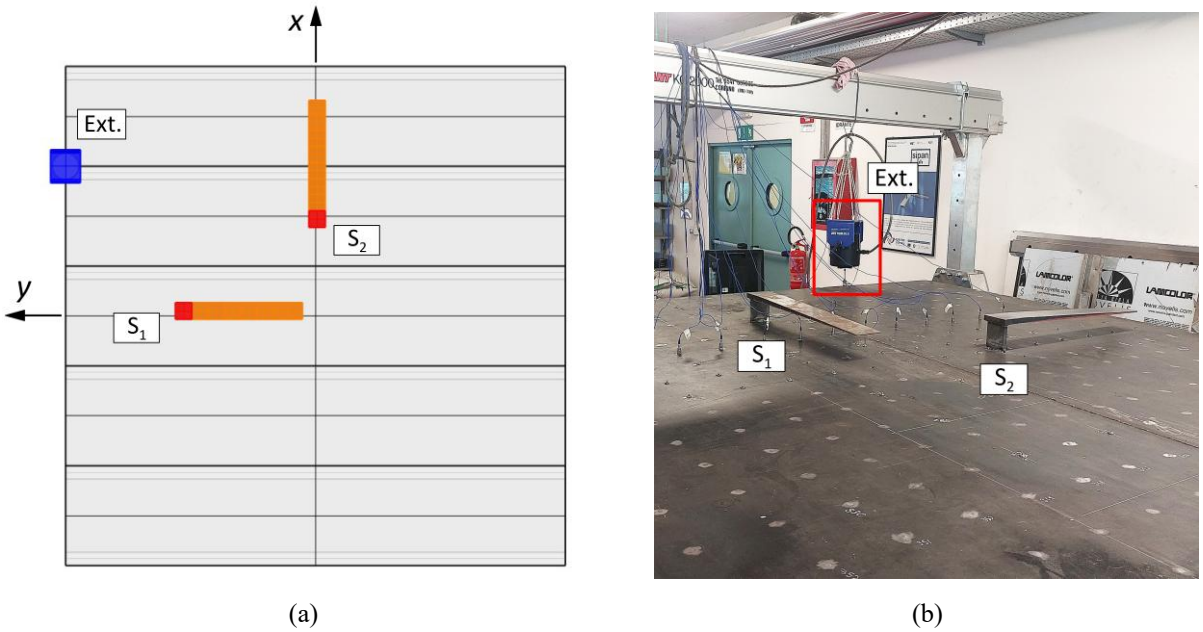

(a) (b)

Fig. 7 a) Positions of the two ABHs and the shaker on the mock-up; b) experimental set-up

Figures 8-13 show the SI field calculated on the mock-up when the excitation is located in (900, 1500, 0), as shown in Figure 7. The amplitude of the exciting force was set to 10^{-3} N, therefore the SI field for the shell elements is displayed in W/mm (the model is in mm/t/s)[1]. Figures 8-10 show the effect of the ABH in position S_1. These cases are characterised by local modes of the sub-panels, as can be observed by the clear lobes on each of them. The ABH, located on the central sub-panel, suppresses the vibration of the entire plating, extracting the vibrational energy, as highlighted by the right-side figures.

[1] The values of Si are indicated in the standard NASTRAN notation, *i.e.* 5.0-0.9 equals to $5.0 \cdot 10^{-9}$

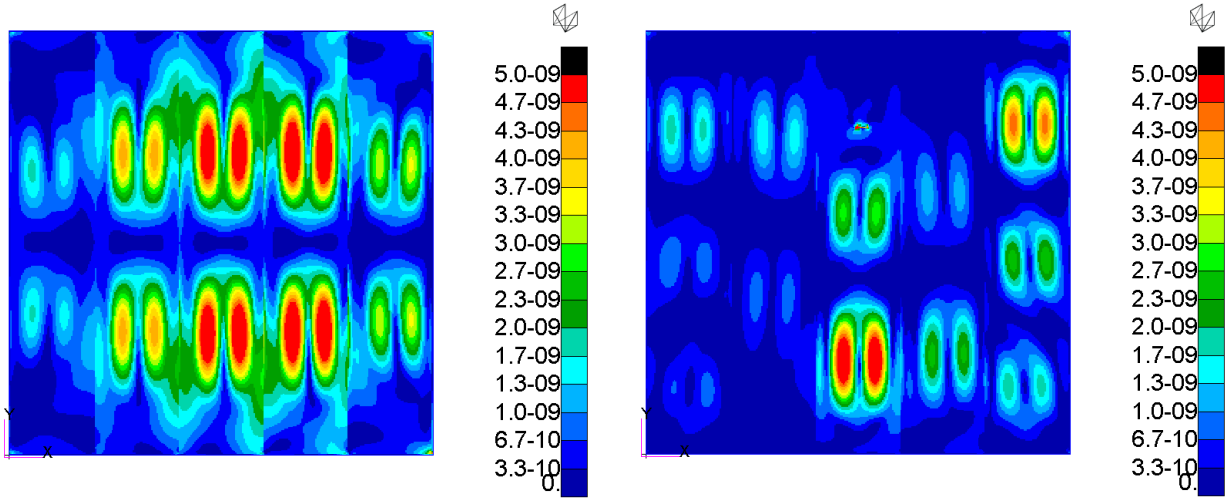

(a) (b)

Fig. 8 SI field at 72.5 Hz (W/mm): a) No ABH b) ABH in S_1

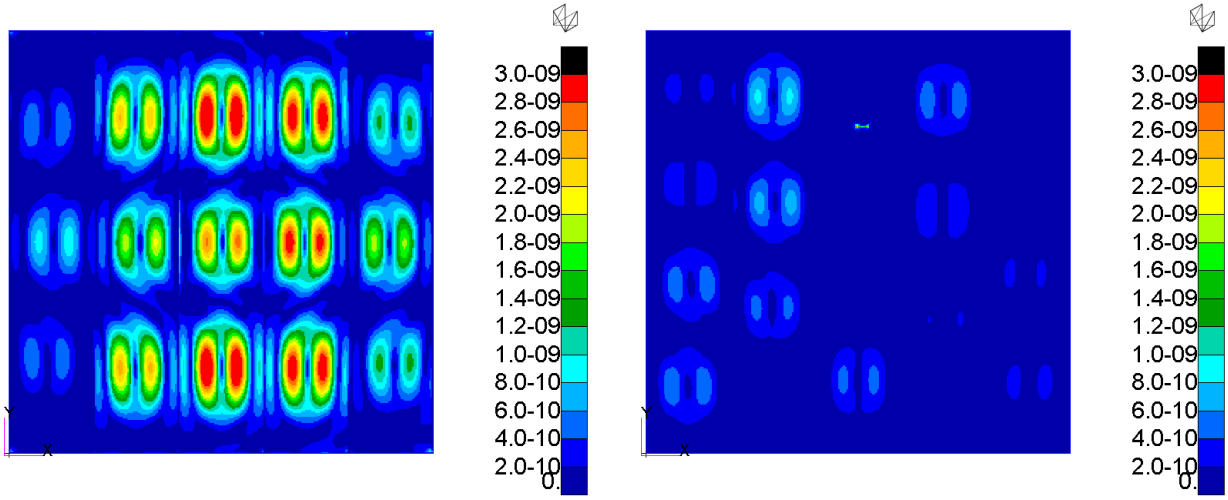

(a) (b)

Fig. 9 SI field at 83.4 Hz (W/mm): a) No ABH b) ABH in S_1

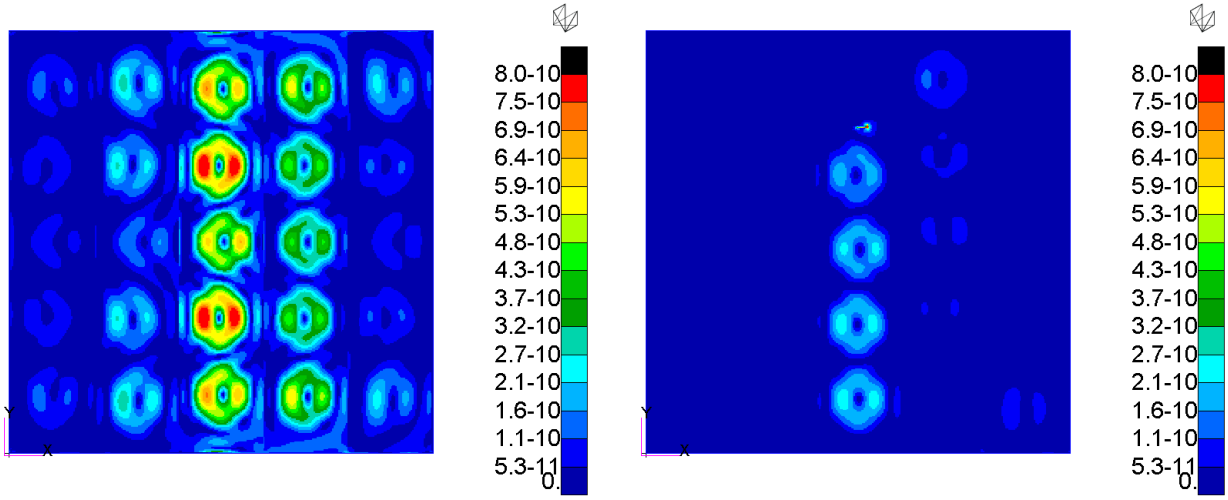

(a) (b)

Fig. 10 SI field at 103.0 Hz (W/mm): a) No ABH b) ABH in S_1

When the deformation involves two or more sub-panels developing orthogonally to the longitudinal direction of the stiffeners (global modes), ABH in position S_1 has a limited effect. The effect of the second ABH calculated by the numerical analysis is illustrated by Figures 11 and 12, which show two examples of the energy decrease obtained (the colour scale is modified to highlight the energy absorption due to the second ABH).

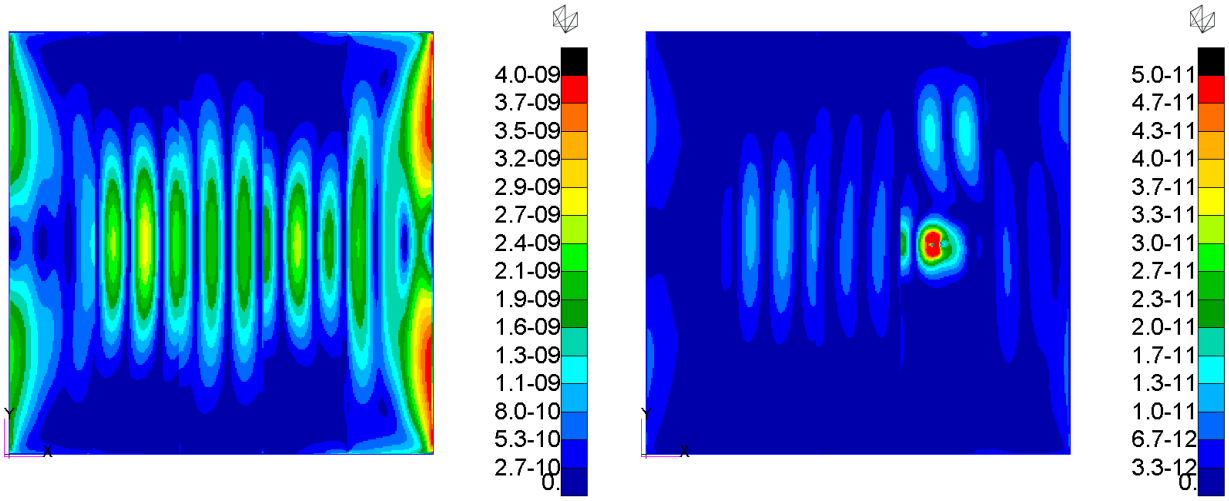

(a) (b)

Fig. 11 SI field at 61.6 Hz (W/mm): a) No ABH b) ABH in S_2

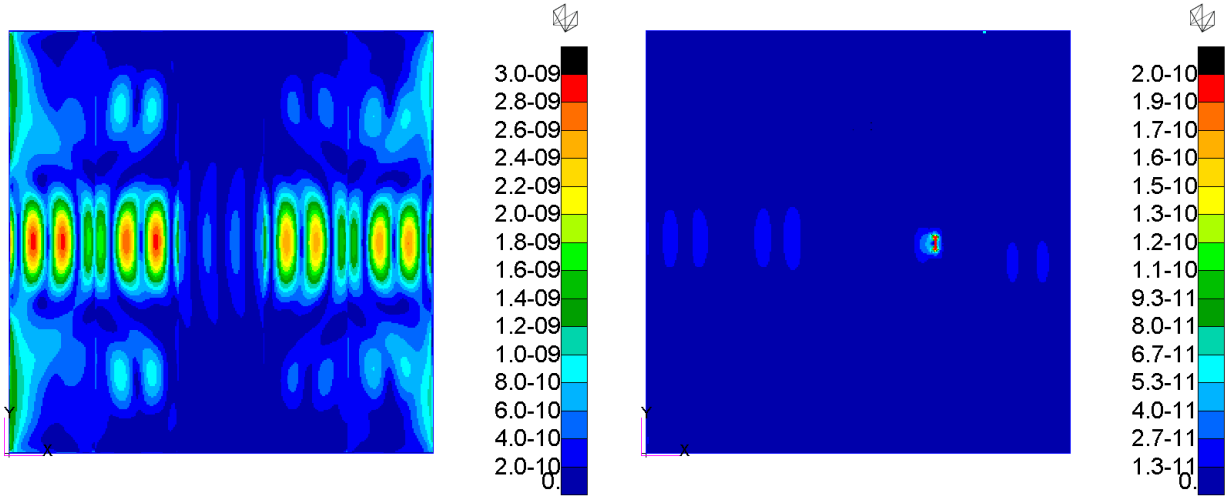

(a) (b)

Fig. 12 SI field at 80.0 Hz (W/mm): a) No ABH b) ABH in S_2

For modes in proximity of the cut-on frequency, the ABH is less effective in dissipating the vibrational energy on the mock-up plating. At 32.2 Hz (Figure 13), the ABH located in position S_2 absorbs some of the energy; however, the absorption is not enough to suppress the mode entirely. This outcome happens for three reasons: i) the ABH damping capacity (inverse of loss factor) is too limited to extract the needed amount of energy from the system; ii) the frequency is below the cut-on frequency, preventing the “black hole” effect to trigger; iii) global modes also involve the stiffeners, which undergo deformation; part of the energy must be also extracted from these elements, whose influence must be considered in the positioning process.

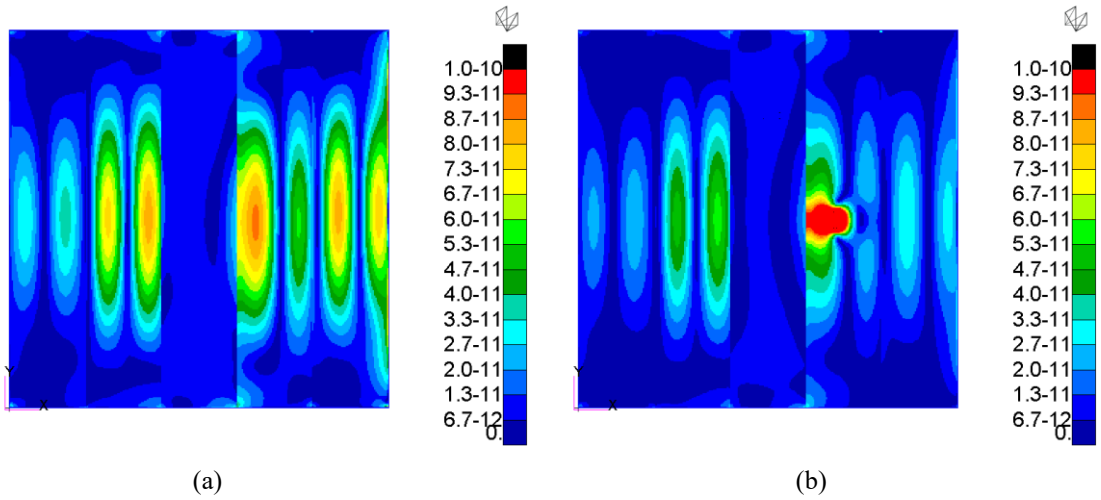

(a) (b)

Fig. 13 SI field at 32.2 Hz (W/mm): a) No ABH b) ABH in S_2

The SI distributions shown in figures from 8 to 13 provide a qualitative idea of the vibrational power level in the stiffened panel plating. It is possible to quantify this power dissipated by the system, by calculating the average input power introduced in the system:

$$\overline{P}_{\text{inj}} = \frac{1}{2}\text{Re}\,(F \cdot v^*) \tag{10}$$

This power is also equal to the average dissipated power over a cycle [73]:

$$\overline{P}_{\text{diss}} = 2\,\omega \sum_{i=1}^{N} ESE_i \cdot \eta_i \tag{11}$$

where F is the applied force, v the velocity in the driving point, ESE is the element strain energy, η is the element loss factor, ω is the frequency, and N is the number of elements considered.

2.5 Experimental setup

The primary objective of the experiments was to verify the ability of the ABHs to reduce the overall vibration of a stiffened panel plating in the low-frequency interval from 0 to 400 Hz, which is typical of machinery on board. Aside from that, secondary objectives were identified in comparing two different connections, welded and screwed, and two different materials, steel and polyacetal, aimed at testing practical solutions for future implementation on board.

Five tests were conducted during the experimental activity; they are summarised in Table 2. ABH Model 1 was used in tests 2 and 3, while in tests 4 and 5, which were designed to investigate different connections and materials, ABH Models 2.1 and 2.2 were used, respectively. The ABH supporting bracket was welded to the mock-up in position S1, and the ABH core was screwed to it.

Table 2 Experimental tests performed on the mock-up

Test number	Label	ABH model	Number of ABH	Position
1	NO ABH	-	0	-
2	ABH1	1	1	S_1
3	ABH12	1	2	S_1 and S_2
4	ABH3	2.1	1	S_1
5	ABH4	2.2	1	S_1

The structure was excited using a PCB Piezotronics 2075E model electrodynamic shaker vertically connected to the mock-up through a steel stinger and a PCB Piezotronics 208C02 Load cell (Figure 14a). The excitation point was located at one of the intersections between primary and secondary beams to distribute the vibrational energy across the structure, as it typically occurs in ship hulls [20]. The structure was excited with a white noise signal controlled with closed-loop feedback using the force signal recorded by the load cell. We used a measurement set made of 441 points equally distributed across the mock-up surface (Figure 4a). Each point, excluding those on the plate's border, was placed at the centre of a 150 x 150 mm square area. Fifteen PCB Piezotronics J352C34 accelerometers were used to record the acceleration. The experimental set-up is shown in Figure 14b. Thirty recording sessions were needed to complete the measurement. The data were acquired for 150 seconds, with a sample rate of 5000 Hz, and processed using a 10 s Hanning window with a superposition of 90 %. The windows were then linearly averaged.

(a) (b)

Fig. 14 Shaker and experimental set up with ABH in position S_1 and S_2

A quantity called Mean Square Velocity (*MSV*) was used to estimate the performance of the ABHs on the mock-up surface. *MSV*, in its general form, is defined as the time and space integral of the squared velocity on a surface S in a period T [74]:

$$MSV = \frac{1}{T}\frac{1}{S}\int_T \int_S v^2(s,t)\ \mathrm{d}s\ \mathrm{d}t \tag{11}$$

The *MSV* is calculated for a discrete number of frequencies or for defined frequency intervals (third-octave bands), for a discrete set of points, and only the vertical component of the speed is used. For a specific frequency ω, the *MSV* is calculated as a double summation as follows:

$$MSV(\omega)=\frac{1}{S}\sum_{n=1}^{N}\sum_{m=1}^{M} v_{nm}^2(\omega)\mathrm{d}S_{nm} \tag{12}$$

where N and M are the total number of points in the x and y directions, dS is the area associated to each nm-the measurement point. For a frequency interval centred in ω_c whose frequency extremes are $\omega_l < \omega_h$, the MSV is obtained by summing up the velocities calculated in the selected interval for each *nm*-th point:

$$MSV(\omega_c)=\frac{1}{S}\sum_{n=1}^{N}\sum_{m=1}^{M}\sum_{\omega_l}^{\omega_h} v_{nm}^2(\omega)\ \mathrm{d}S_{nm} \tag{13}$$

To compare experimental and numerical data, only the *z* component was used, and the velocities were divided by the input force. Therefore, in the context of this paper, the term *MSV* is used to refer to mobility rather than velocity.

3. Results and Discussion

3.1 Vibrational power quantitative comparison

Table 3 shows total dissipated power by the elements of the plating in FE model of the mock-up for the frequencies shown in Figures 8-13.

Table 3 Average dissipated power over a cycle by the plating elements for the examples shown in Section 2.4

f [Hz]	Power dissipated [10^{-9} W]		
	NO ABH	ABH1	ABH2
32.2	0.2	0.2	2.1
61.6	46.4	19.6	2.3
72.5	20.4	3.6	26.4
80.0	11.8	15.9	4.4
83.4	33.8	3.6	13.2
103.0	13.3	1.9	16.8

As the table shows, when one or two ABHs are introduced, the velocity levels measured on the plating decrease, and therefore also the average power dissipated decreases. This outcome may appear counterintuitive, as one may expect the dissipated power to increase adding more dissipative elements. This apparent inconsistency happens because all the tests presented in the paper were carried out using the same input force. This configuration does not correspond to introducing the same input power into the systems, as the power strictly depends on the system dynamics. When the ABH is connected to the plating, the dynamics changes, as well as the power introduced. For this reason, we preferred to provide the quantitative comparison in terms of velocity reduction, rather than power dissipation.

3.2 Narrowband Analysis

The effect of the two ABHs on the mock-up was analysed by computing the mode shapes at different frequencies using the 441 accelerometer signals acquired for each condition. Figure 15 shows the narrowband *MSV* between 10 and 110 Hz. The coloured areas highlight the differences obtained between the conditions of NO ABH and ABH1 (light colours), and ABH1 and ABH12 (dark). The blue areas indicate a positive gain, while red areas indicate a negative one. The ABHs start working around 30 Hz; the first peak affected is at 28.8 Hz. This outcome was expected since the cut-on frequency selected was 30 Hz. However, the ABH mitigation below 50 Hz is limited; above this frequency, many peaks are damped or eliminated due to the ABH, with local *MSV* differences up to 30 dB (five times the original value).

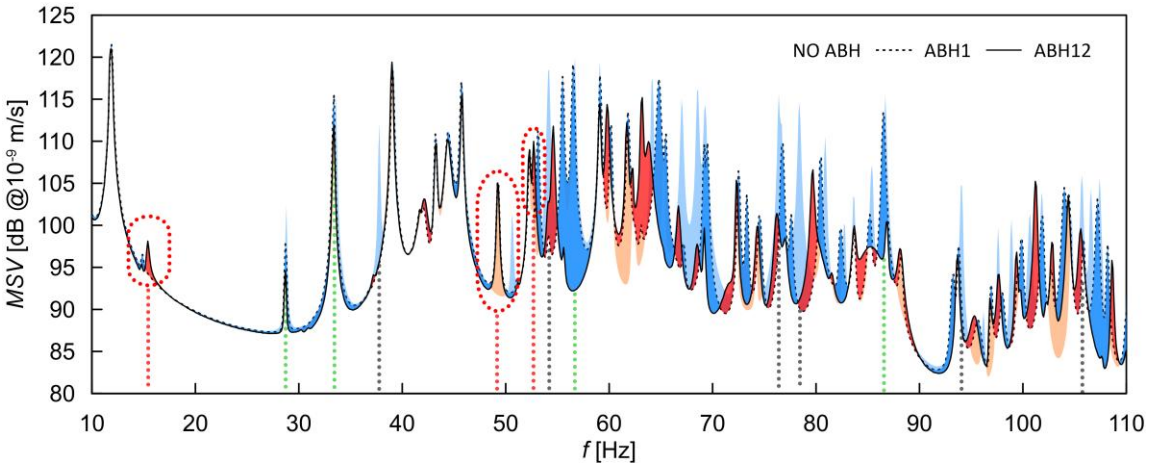

Fig. 15 *MSV* comparison between configurations NO ABH; ABH1, and ABH12

Some deformations were selected to illustrate the effect of the ABHs on the structure; they are indicated in Figure 15 by vertical dotted lines. Figure from 16 to 25 show the vertical deformation of the mock-up computed using the signals measured by the 441 accelerometers distributed on the plating. The number on the colour bar indicates an acceleration (using the displacements, the deformations would be visually the same, but with the phase reversed), which was normalised using the input force ($m/s^2/N$). Unlike the numerical results in Sec. 2.4, where the shape of the modes is clearly visible, real deformations often show an overlapping of modes. Figures 16-21 show six deformations characterised by a number of lobes from one to eight. The figures labelled as (a) refer to the case with NO ABH, those labelled as (b) refer to the case ABH1. The grey dotted lines indicate these modes in Figure 15. For some cases, the two colour spectra used are different to allow the deformation to be visible after the ABH installation.

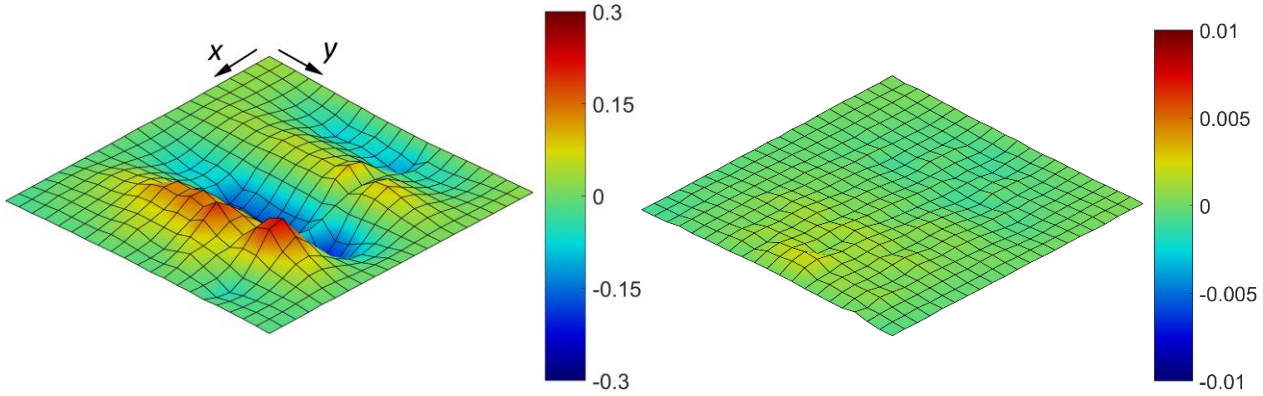

(a) (b)

Fig. 16 One-lobe local deformation at 37.8 Hz: a) NO ABH b) ABH1 (Frame of reference given in Figure 4c is shown in the upper corner and is valid for all figures from 16 to 26)

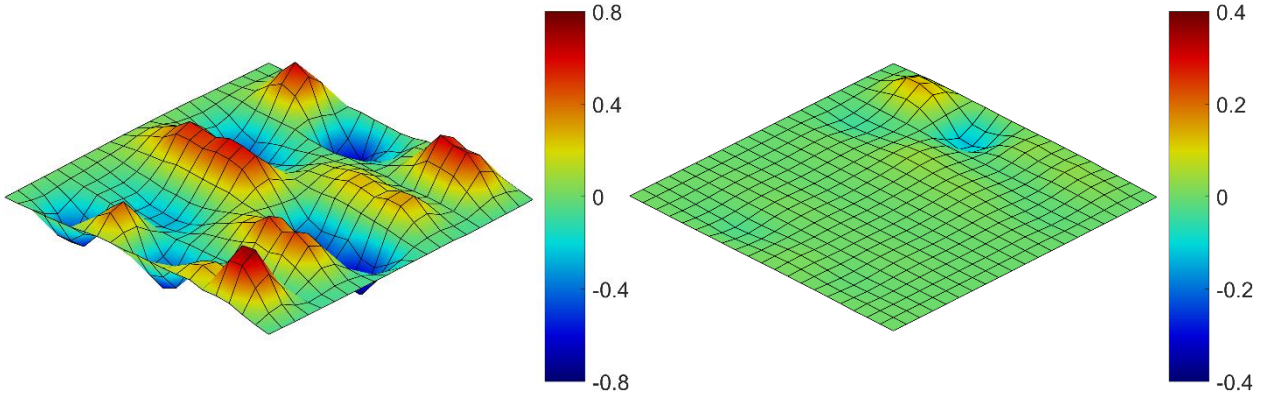

(a) (b)

Fig. 17 Mixed two-three lobe local deformation at 54.2 Hz: a) NO ABH b) ABH1

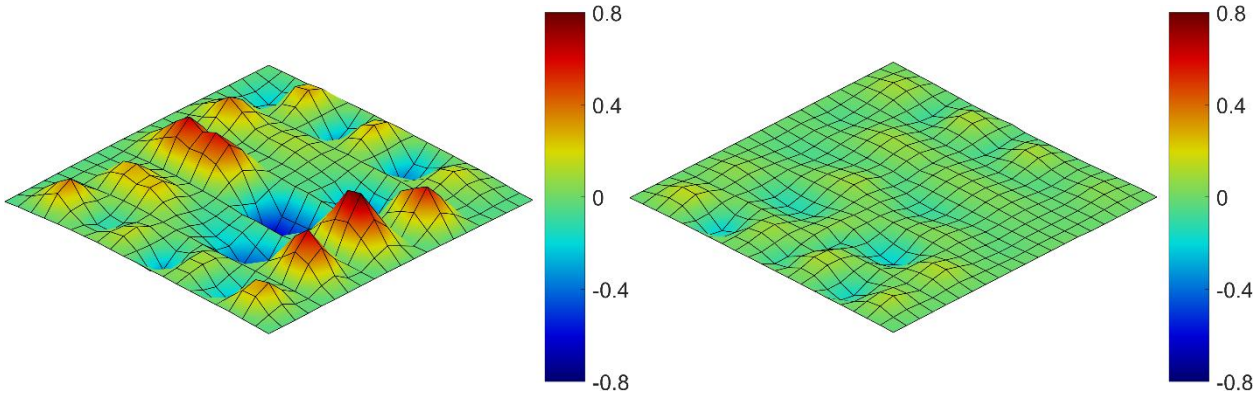

(a) (b)

Fig. 18 Mixed three-four lobe local deformation at 76.4 Hz: a) NO ABH b) ABH1

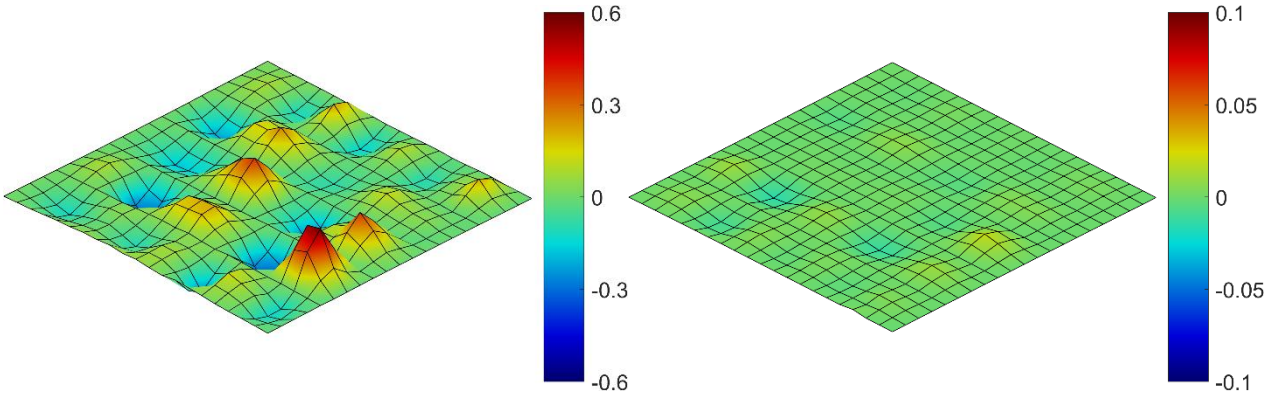

(a) (b)

Fig. 19 Mixed four-five lobe local deformation at 78.3 Hz: a) NO ABH b) ABH1

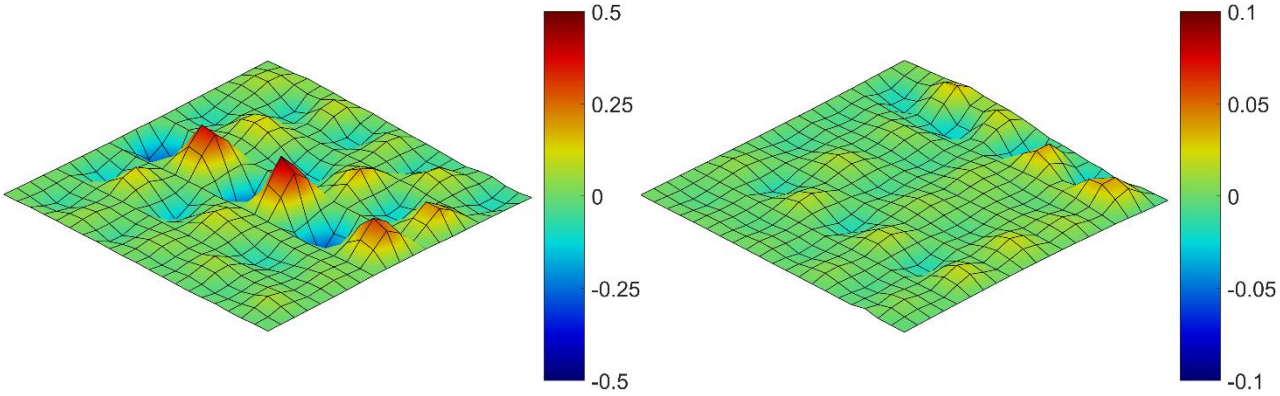

(a) (b)

Fig. 20 Six-lobe local deformation at 94.1 Hz: a) NO ABH b) ABH1

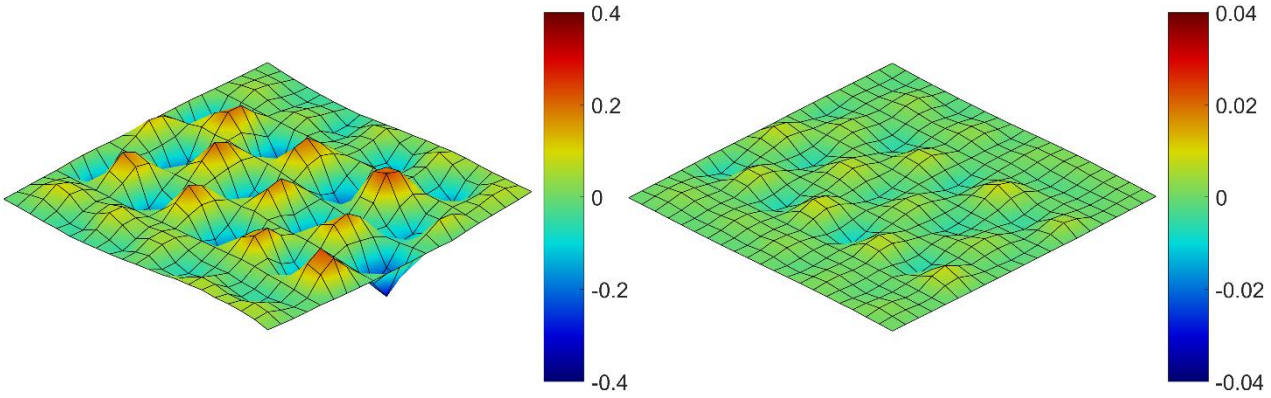

(a) (b)

Fig. 21 Mixed seven-eight lobe local mode at 106.6 Hz: a) NO ABH b) ABH1

Figures 22-25 report the vibration pattern at 28.8, 33.6, 56.7, and 86.7 Hz. These are global modes indicated in Figure 15 by green dotted lines. In this case, since they are affected by the ABH in position S2, the figures labelled as (a) refer to the case with NO ABH, those labelled as (b) refer to the case ABH12.

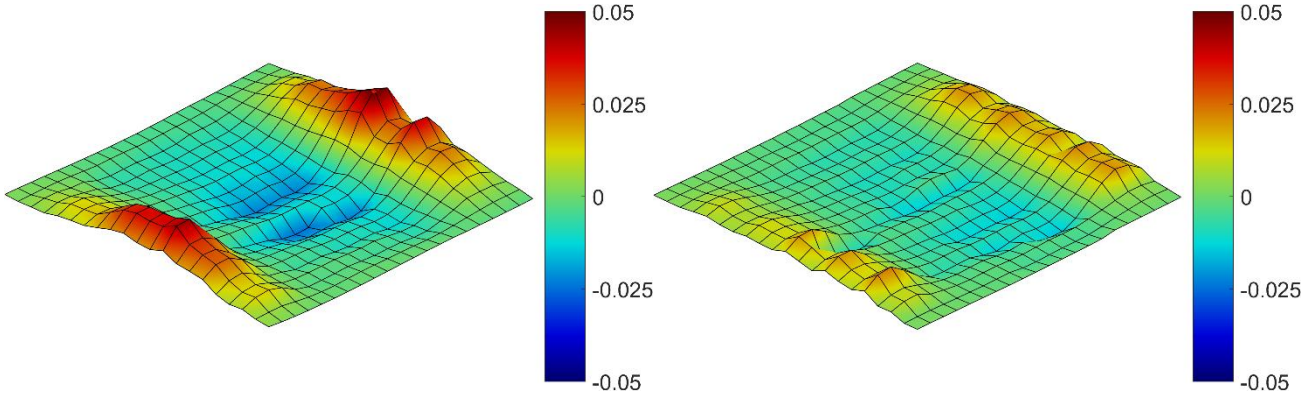

(a) (b)

Fig. 22 Global deformation at 28.8 Hz: a) NO ABH b) ABH12

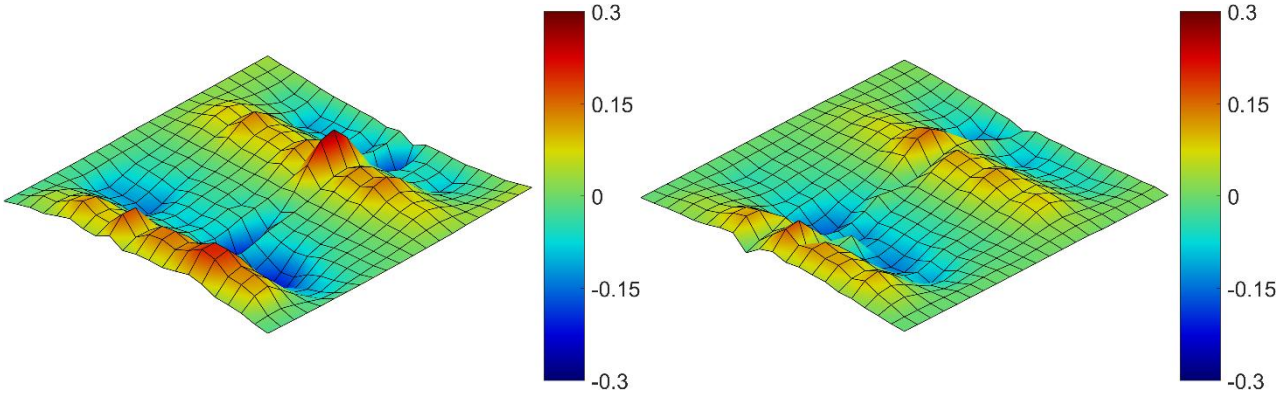

(a) (b)

Fig. 23 Global deformation at 33.4 Hz: a) NO ABH b) ABH12

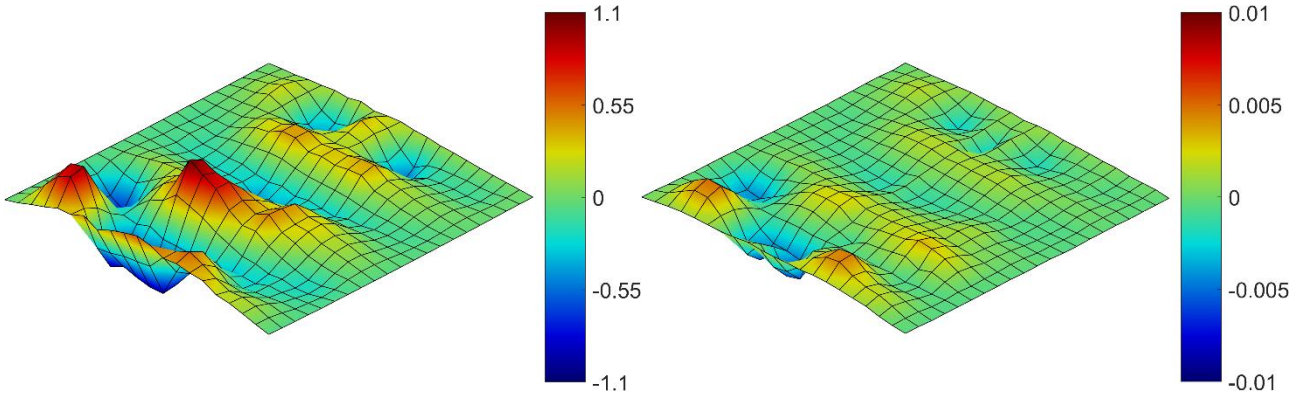

(a) (b)

Fig. 24 Global deformation at 56.7 Hz: a) NO ABH b) ABH12

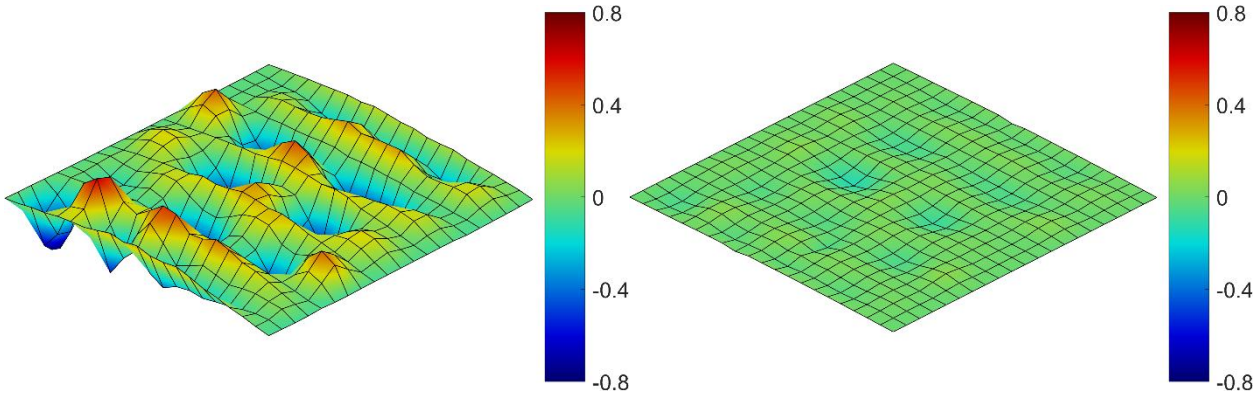

(a) (b)

Fig. 25 Global deformation at 86.7 Hz: a) NO ABH b) ABH12

In some cases, the ABHs have a negative impact on the global response, introducing additional peaks, like those at 14.8, 15.4, 49.2, and 54.6 Hz, indicated by the red dotted circles in Figure 15. These peaks are generated by rigid modes of the ABH beam oscillating around the junction with the vertical support, so their effect is localised near the connection between ABH and the mock-up (Figure 26). The impact of these modes on the global response depends on the relative dimension of the two systems involved. In our case, since the ABH weight is around 1 % of the mock-up total weight, the amplitude of the generated peaks is lower than the amplitudes of the main peaks characterising the structure's response. These undesired effects are unavoidable when the ABH is welded to the support; using a less rigid support would decrease the transmission of the vibration to the underneath host structure. Solution ABH3, where the ABH is screwed to the support, does not show the 14.8 Hz peak, while the amplitude of the 49.2 Hz peak is reduced. Another option is to relegate these peaks to frequency ranges that are not critical for the operation of the structure or combining different ABHs whose mitigation effect may mutually compensate for the disadvantage.

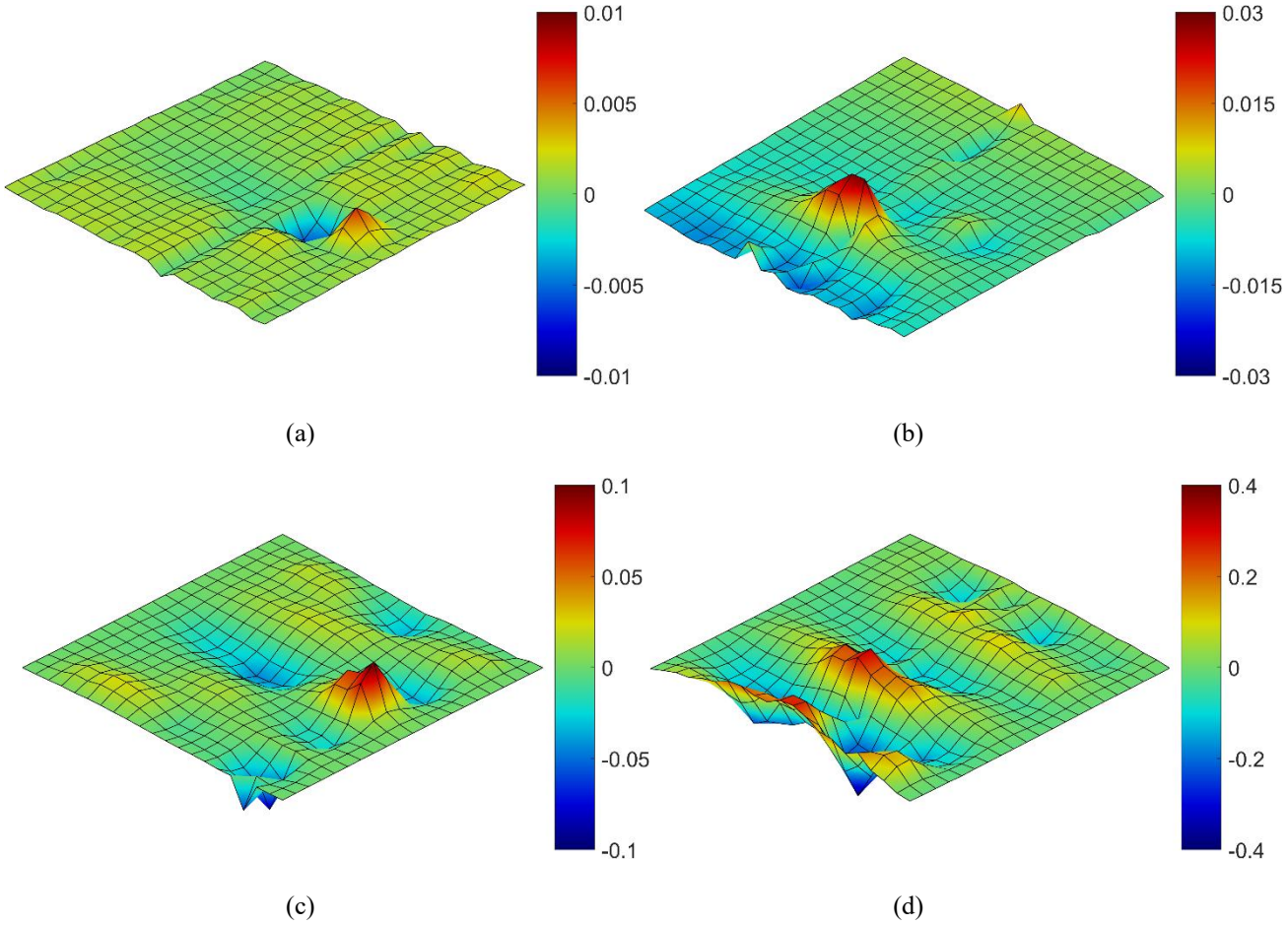

Fig. 26 Induced deformations due to the ABH oscillating rigidly around the support junction: a) 14.8 Hz b) 15.4 Hz c) 49.2 Hz d) 54.6 Hz

3.3 Broadband Analysis

The narrowband transfer *MSV* function is useful for seeing the effect of the ABHs on the peaks. However, as frequency increases, the punctual visualisation of the peak suppression starts to be more challenging. The mode density increases and the system's dynamic is dominated by many overlapping modes, mostly "local" ones, characterised by a high number of lobes. To visualise the effect of energy absorption, the *MSV* was computed for the third-octave bands between 40 and 400 Hz.

Figure 27 shows the third-octave bands *MSV* level differences between the conditions of NO ABH and ABH1, and NO ABH and ABH12. The first ABH leads to an average improvement of the *MSV* third-octave band gains of 1.4 dB. Adding the second ABH improves the reduction achieved in each of the third-octave bands investigated by another 1.4 dB, on average. The maximum reduction is obtained in correspondence with the 80 Hz third-octave bands, as many of the peaks in that band are suppressed or reduced. The gain obtained is 6.6 dB, meaning that the *MSV* was reduced to one fourth of the original value. In the 50, 63, 125, 160, 200 Hz third octave bands, the *MSV* is around half of the original value. The 40 Hz third-octave band gain is null as the ABH is ineffective on the main peaks, since the cut-on frequency is 30 Hz. In the 100 Hz third-octave band, while the first ABH leads to a gain which is aligned with those in the other intervals, the second ABH does not add any substantial effect. In the 100 Hz band interval (from 89 to 112 Hz), although in general most of the peaks are reduced by the ABHs, the maximum peak amplitude goes from 106 dB with no ABHs installed to 105.2 dB when two ABHs are installed. Since third-octave band *MSV* levels are dominated by the maximum amplitudes, the total gain is then limited to 1.8 dB.

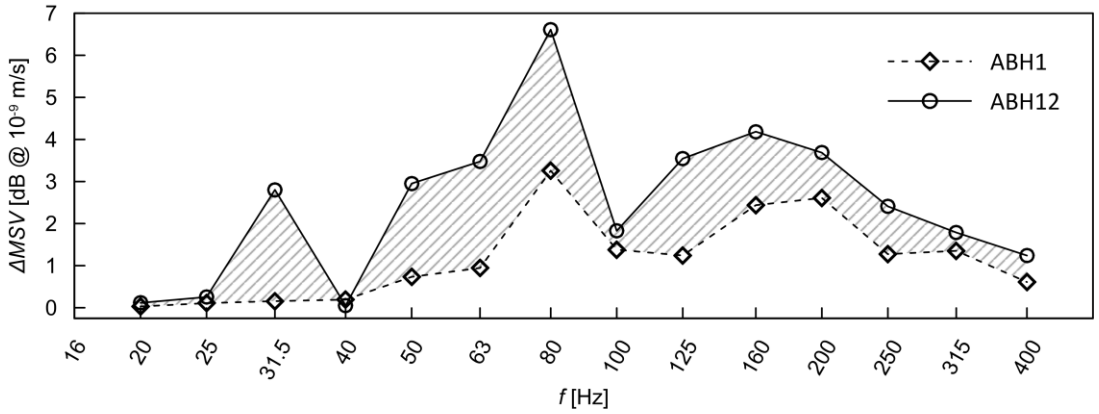

Fig. 27 Third octave band *MSV* differences between the case NO ABH and ABH1 and ABH12

When frequency increases over 200 Hz, the vibration reduction due to both ABHs progressively decreases, indicating a less effective impact of the two ABHs. Since the vibrational energy is more distributed on the mock-up plating due to the increased mode density, it is more important to tackle more modes by placing more ABHs in strategic positions, since each ABH works effectively only on the modes having high energy in its location. Moreover, a low cut-on frequency is not needed for high frequencies; more small-sized ABHs, rather than fewer but longer ABHs, are expected to be advantageous.

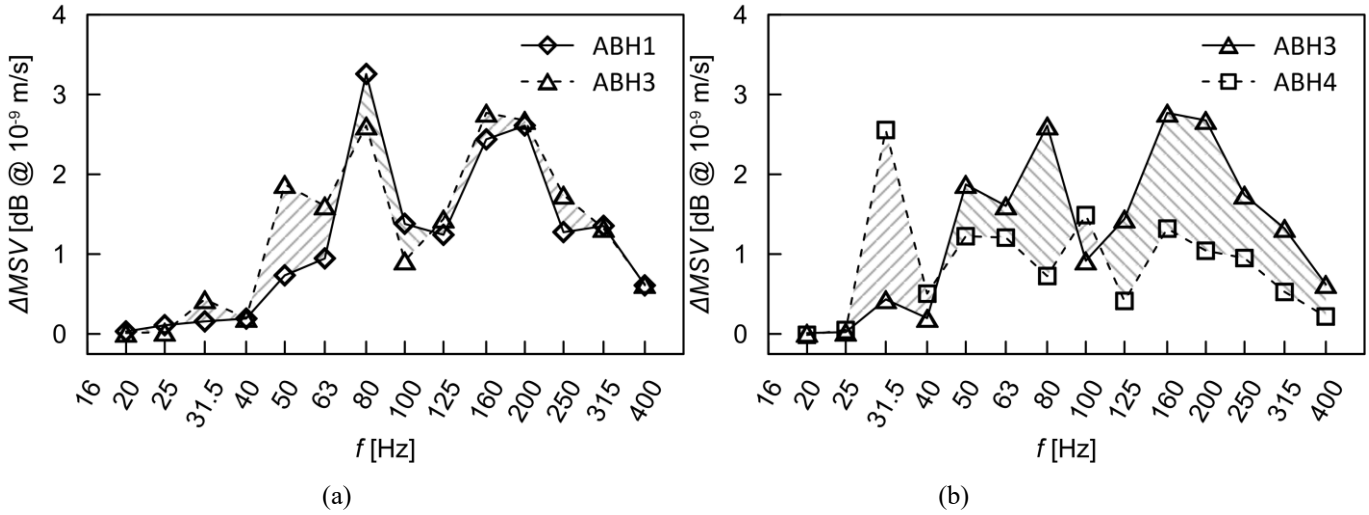

Fig. 28 Third octave band *MSV* differences between the case NO ABH and: a) ABH1 and ABH3 and b) ABH3 and ABH4

Conditions ABH1 (welded) and ABH3 (screwed) gave very similar results, especially over 80 Hz (0.3 dB difference on average). This result indicates no significant difference in using the welded or the screwed supporting bracket, with the latter giving slightly better results in the 50 and 63 Hz third-octave bands and over 125 Hz. Configuration ABH4 is the only configuration that shows a small gain in the 40 Hz third-octave band due to the lower cut-on frequency (8.5 Hz against 30 Hz). The polyacetal ABH vibration decrease capacity is lower compared with the steel one in all the third-octave bands over 40 Hz, except the 100 Hz one. The polymer ABH resorts only to its internal damping, which is lower than that of the steel with VEM application. The possibility of applying a damping layer to increase the dissipation of the polyacetal ABH may be investigated in future.

3.4 Cumulative results

Figure 29 shows the cumulative *MSV* gains calculated between 18 and 450 Hz (corresponding to the third-octave bands from 20 to 400 Hz) for each of the five sub-panels of the mock-up. Each colour corresponds to a different testing condition as indicated by the legend. A few observations can be made by analysing the picture: the panel showings the main decrease of *MSV* level is the central panel P3, where most of the energy is absorbed by the ABH in position S1; the ABH in position P1 mostly affects panels P3, P4, and P5, as the

energy propagating from the excitation point towards these panels is intercepted by the ABH; the effect of the first ABH on panels P1 and P2 is limited; the ABH in position P2 has an impact on all five sub-panels (it acts on global modes), however its effectiveness tends to decrease moving away from position S2 (differences between ABH12 and ABH1 in Figure 29); the results observed in Figure 28 are confirmed: the screwed solution works slightly better than the welded one, the polyacetal resin ABH has a limited effect compared with the steel one.

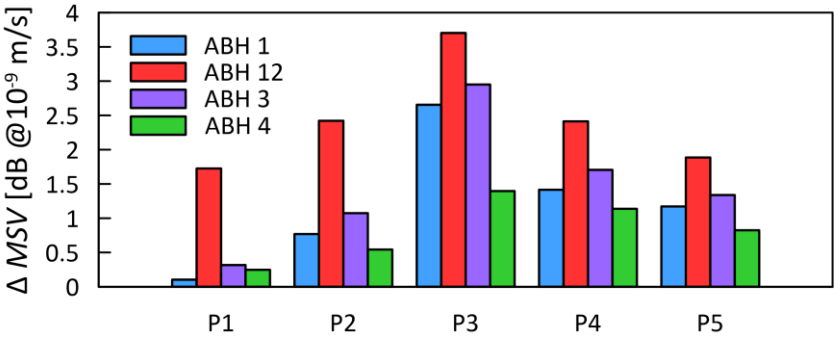

Fig. 29 Overall *MSV* differences between the case NO ABH and the other configurations obtained for each mock-up sub-panel for the interval 18 - 450 Hz

Table 4 Overall *MSV* levels and gains obtained for the entire mock-up for the interval 18 ÷ 450 Hz

	MSV [dB]	Δ*MSV* [dB]
NO ABH	137.3	-
ABH1	136.1	1.1
ABH12	134.9	2.4
ABH3	135.9	1.4
ABH4	136.5	0.8

The cumulative *MSV* levels for all the mock-up plating were also calculated, and they are shown in Table 4. The overall differences between NO ABH and the other testing conditions are also reported. The ABH in position S2 has a major impact on the overall response of the mock-up, leading to a gain more than double that obtained by the only ABH in position S1.

3.5 Final Considerations

The application of Acoustic Black Holes on the mock-up reduces the *MSV* in the range from 40 to 400 Hz. The gains obtained reach up to 6.6 dB in some third-octave bands and up to 30 dB when single peaks are considered. This highlights the great potential for decreasing the vibrations if specific, limited target frequency intervals are properly selected, since the vibration reduction depends on the modes suppressed.

These conclusions can be generalized to different frequency ranges of interests. At low frequencies, where ship structures are particularly difficult to treat, the ABH geometry must be properly scaled. Longer and wider ABHs may be required, which can conflict with space constraints and structural requirements. Moreover, at these frequencies, the structural deformations also involve rigid stiffeners; thus, ABH position must be selected with respect to the combined deformation pattern of plating and stiffening elements. At higher frequencies, performance can be enhanced by increasing the number of ABHs while reducing their size. The positioning approach must be modified to consider a higher number of ABHs: the use of repeated patterns may be a suitable option, without resorting to case-by-case analyses to select the ABH locations.

Alternative strategies for connecting ABHs to the host structure may prove advantageous. Less rigid coupling at the interface could improve vibration attenuation and simplify integration, but this needs careful analysis, as a connection that is too weak could compromise efficiency. Different materials can also be used. Lighter or polymer-based ABHs could facilitate installation and lower the effective cut-on frequency for the same taper length. However, using non-metallic materials on board ships introduces additional constraints

related to safety (fire resistance, smoke and toxicity emissions, and compliance with the FTP Code). These requirements may limit the theoretical advantages of polymers. Polymer-based structures have intrinsic damping; however, it would probably need to be increased to match the performance of the steel–VEM sample. A further complication is represented by adhesion: it is unclear whether conventional VEM layers bond effectively to polymer substrates.

4. Conclusion

This paper presents an application of ABHs on a stiffened panel, a base unit element of a ship hull from a vibrational point of view, with the goal of mitigating the hull structural vibration in the low-frequency range (below 400 Hz). It was shown that ABH integration can be performed aiming at reducing specific peaks or the energy in broader frequency ranges. The study was performed experimentally on a mock-up, representing a typical ship stiffened panel. Two ABHs were installed; the first one suppressed mainly local modes of the sub-panels, the second ABH tackled the global modes involving the structure entirely and was intended to be complementary to the first one installed. The ABHs proved to be an alternative solution to traditional vibration reduction systems used on ships. This paper aimed to take a step towards increasing the TRL of the ABH application on marine structures, initially estimated 3-4.

Future steps for implementing ABHs on board would require feature optimisation to adapt the device to different operative ranges, comparison with existing solutions already used in ship structures, and testing in operational real-case scenarios. Targeting very low frequencies implies dimensions that could make it challenging to integrate the device onboard without interfering with components and systems. Different geometries and alternative materials could compensate for this disadvantage. More compact shapes may provide comparable energy trapping in less space, making them better suited to constrained shipboard environments.

FUNDING

Results achieved with the funding obtained under the Axis IV of PON Research and Innovation 2014-2020 “Education and research for recovery – REACT-EU”.

This work was also supported by the European Union – European Regional Development Fund (ERDF), Friuli Venezia Giulia PR FESR 2021-2027, CUP J93C23002420005 – Project “Silentship- Acoustic Black Holes, nuova frontiera per navi silenziose”.

ACKNOWLEDGMENTS

We acknowledge the support of FRA-Fondi Ricerca di Ateneo, FRA 2025.

REFERENCES

[1] Yokota, S., 1906. On vibration of steamers. *Proceedings of the Tokyo Mathematico-Physical Society*, 3(5), 91-102. https://doi.org/10.11429/subutsugaiyo1903.3.91

[2] Scientific American, 1907. Vibration in passenger ships. *Scientific American*, 97(26), 470-471. https://doi.org/10.1038/scientificamerican12281907-470c

[3] Akimoff, N.W., 1922. Vibration in ships. *The Society of Naval Architects of Japan*.

[4] Parunov, J., Pestelli, C., Rudan., S., Hadžić, N., Senjanović., I. 2012. Review of Methods for Structure Born Noise Prediction on Ships. *Brodogradnja*, 63(2), 134-139.

[5] Cho, D.S., Kim, K.S., Kim, B., 2010. Structural intensity analysis of a large container carrier under harmonic excitations of propulsion system. *International Journal of Naval Architecture and Ocean Engineering*, 2, 87-95. https://doi.org/10.2478/IJNAOE-2013-0023

[6] Tang., H., Fu, B., Yang, Y., Wan, Q. 2026. Fault diagnosis and restoration of ship structure monitoring signals based on machine learning. *Brodogradnja*, 77(3), 77301. https://doi.org/10.21278/brod77301

[7] Peric, M. Prediction of Cavitation on Ships. 2022. *Brodogradnja*, 73(3), 39-58. https://doi.org/10.21278/brod73303

[8] Nilsson, A., Liu, B., 2015. Vibro-acoustics, volume 2. *Springer*, Berlin. https://doi.org/10.1007/978-3-662-47934-6

[9] Park, M.H., Yeo, S., Choi, J.H., Lee, W.J., 2024. Review of noise and vibration reduction technologies in marine machinery: Operational insights and engineering experience. *Applied Ocean Research*, 152, 104195. https://doi.org/10.1016/j.apor.2024.104195

[10] Avi, E., Laakso, A., Romanoff, J., Remes, H., Lillemäe-Avi, I., 2021. Coarse mesh finite element model for cruise ship global and local vibration analysis. *Marine Structures*, 79, 103053. https://doi.org/10.1016/j.marstruc.2021.103053

[11] Orrenius, U., Finnveden, S., 1996. Calculation of wave propagation in rib-stiffened plate structures. *Journal of Sound and Vibration*, 198(2), 203-224. https://doi.org/10.1006/jsvi.1996.0565

[12] Senjanović., I., Tomasević, S., Grubišić, R. 2007. Coupled Horizontal and Torsional Vibrations of Container Ships. *Brodogradnja*, 58(4), 365-379.

[13] Yin Y., Cui, H., Zhao, D., Hong, M. 2014. Predicting Method of Natural Frequency for Ship's Overall Vertical Vibration. *Brodogradnja*, 65(3), 49-58.

[14] Avi, E., Lillemäe, I., Romanoff, J., Niemelä, A., 2015. Equivalent shell element for ship structural design. *Ships and Offshore Structures*, 10(3), 239-255. https://doi.org/10.1080/17445302.2013.819689

[15] Clarkson, B.L., Ford, R.D., 1962. The response of a typical aircraft structure to jet noise. *Journal of the Royal Aeronautical Society,* 66(613), 31-40. https://doi.org/10.1017/S0001924000063399

[16] Nilsson, A.C., 1978. Reduction of structure-borne sound in simple ship structures: Results of model tests. *Journal of Sound and Vibration*, 61(1), 45-60. https://doi.org/10.1016/0022-460X(78)90040-8

[17] Nilsson, A.C., 1984. A method for the prediction of noise and velocity levels in ship constructions. *Journal of Sound and Vibration*, 94(3), 411-429. https://doi.org/10.1016/S0022-460X(84)80020-6

[18] Xu, X.D., Lee, H.P., Wang, Y.Y., Lu, C., 2004. The energy flow analysis in stiffened plates of marine structures. *Thin-Walled Structures*, 42, 979-994. https://doi.org/10.1016/j.tws.2004.03.006

[19] Cho, D.S., Choi, T.M., Kim, J.H., Vladimir, N., 2018. Dominant components of vibrational energy flow in stiffened panels analysed by the structural intensity technique. *International Journal of Naval Architecture and Ocean Engineering*, 10(5), 583-595. https://doi.org/10.1016/j.ijnaoe.2017.11.003

[20] Kong, D., Zhang, X., Lu, B., Li, C., Liu, Y., 2023. Identifying dominant components of vibrational energy flow in U-rib plates of bridge based on structural intensity. *Journal of Low Frequency Noise, Vibration and Active Control*, 42(1), 192-208. https://doi.org/10.1177/14613484221122732

[21] Fragasso, J., Moro, L., 2022. Structure-borne noise of marine diesel engines: Dynamic characterization of resilient mounts. *Ocean Engineering*, 261, 112116. https://doi.org/10.1016/j.oceaneng.2022.112116

[22] Sun, Y., Wu, T., Su, Y., Peng, H. 2020. Numerical Prediction on Vibration and Noise Reduction Effects of Propeller Boss Cap Fins on a Propulsion System. *Brodogradnja*, 71(4), 1-18. https://doi.org/10.21278/brod71401

[23] Turner, A.E., 1969. The use of damping materials for noise reduction on a passenger ship. *Journal of Sound and Vibration*, 10(2), 187-197. https://doi.org/10.1016/0022-460X(69)90195-3

[24] Nilsson, A.C., 1977. Attenuation of structure-borne sound in superstructures on ships. *Journal of Sound and Vibration*, 55(1), 71-91. https://doi.org/10.1016/0022-460X(77)90584-3

[25] Chen, D., Li, Y., Gong, Y., Li, X., Ouyang, W., Li, X., 2024. Low frequency vibration isolation characteristics and intelligent design method of hull grillage metastructures. *Marine Structures*, 94, 103572. https://doi.org/10.1016/j.marstruc.2023.103572

[26] Li, X., Hu, Y., Li, Y., 2025. Analytical study and multi-objective optimization of low-frequency flexural vibration band gaps of periodic orthogonal stiffened meta-plates. *Marine Structures*, 103, 103837. https://doi.org/10.1016/j.marstruc.2025.103837

[27] Smith, T.A., Rigby, J., 2022. Underwater radiated noise from marine vessels: A review of noise reduction methods and technology. *Ocean Engineering*, 266, 112863. https://doi.org/10.1016/j.oceaneng.2022.112863

[28] Mironov, M.A., 1988. Elastic wave propagation in a plate, thickness of which smoothly decreases to zero on a finite interval. *Akusticheskii Zhurnal*, 34, 546-547.

[29] Krylov, V.V., 2014. Acoustic black holes: Recent developments in the theory and applications. IEEE Transactions on Ultrasonics, Ferroelectrics, *and Frequency Control*, 61, 1296-1306. https://doi.org/10.1109/TUFFC.2014.3036

[30] Conlon, S.C., Fahnline, J.B., Semperlotti, F., 2015. Numerical analysis of the vibroacoustic properties of plates with embedded grids of acoustic black holes. *Journal of the Acoustical Society of America*, 137, 447-457. https://doi.org/10.1121/1.4904501

[31] Feurtado, P.A., Conlon, S.C., 2016. An experimental investigation of acoustic black hole dynamics at low, mid, and high frequencies. *Journal of Vibration and Acoustics*, 138. https://doi.org/10.1115/1.4033894

[32] Feurtado, P.A., Conlon, S.C., 2017. Transmission loss of plates with embedded acoustic black holes. *Journal of the Acoustical Society of America*, 142, 1390-1398. https://doi.org/10.1121/1.5001503

[33] Du, X., Huang, D., Fu, Q., Zhang, J., 2019. Effects of acoustic black hole parameters and damping layer on sound insulation performance of ABH circular plate. *Applied Sciences*, 9, 5366. https://doi.org/10.3390/app9245366

[34] Deng, J., Guasch, O., Maxit, L., Zheng, L., 2021. Transmission loss of plates with multiple embedded acoustic black holes using statistical modal energy distribution analysis. *Mechanical Systems and Signal Processing*, 150, 107262. https://doi.org/10.1016/j.ymssp.2020.107262

[35] Zhou, T., Cheng, L., 2018. A resonant beam damper tailored with acoustic black hole features for broadband vibration reduction. *Journal of Sound and Vibration*, 430, 174-184. https://doi.org/10.1016/j.jsv.2018.05.047

[36] Li, M., Deng, J., Zheng, L., Xiang, S., 2022. Vibration mitigation via integrated acoustic black holes. *Applied Acoustics*, 198, 109001. https://doi.org/10.1016/j.apacoust.2022.109001

[37] Wen, H., Guo, X., Ma, R., Guo, J., Shi, Z., Ye, L., 2024. Vibration control mechanisms of plate structures by 1D acoustic black hole dynamic vibration absorber. *Physica Scripta*, 99(5), 055268. https://doi.org/10.1088/1402-4896/ad3e39

[38] Ji, H., Wang, N., Zhang, C., Wang, X., Cheng, L., Qiu, J., 2021. A vibration absorber based on two-dimensional acoustic black holes. *Journal of Sound and Vibration*, 500, 116024. https://doi.org/10.1016/j.jsv.2021.116024

[39] Ji, H., Zhao, X., Wang, N., Huang, W., Qiu, J., Cheng, L., 2022. A circular eccentric vibration absorber with circumferentially graded acoustic black hole features. *Journal of Vibration and Acoustics*, 144. https://doi.org/10.1115/1.4053475

[40] Zhao, X., Wang, C., Ji, H., Qiu, J., Cheng, L., 2024. Vibration reduction by a partitioned dynamic vibration absorber with acoustic black hole features. *Chinese Journal of Mechanical Engineering*, 37, 75. https://doi.org/10.1186/s10033-024-01049-x

[41] Lee, J.Y., Jeon, W., 2017. Vibration damping using spiral acoustic black holes. *Journal of the Acoustical Society of America*, 141(3), 1437-1450. https://doi.org/10.1121/1.4976687

[42] Lee, J.Y., Jeon, W., 2021. Wave-based analysis of the cut-on frequency of curved acoustic black holes. *Journal of Sound and Vibration*, 492, 115731. https://doi.org/10.1016/j.jsv.2020.115731

[43] Park, S., Lee, J.Y., Jeon, W., 2022. Vibration damping of plates using waveguide absorbers based on spiral acoustic black holes. *Journal of Sound and Vibration*, 521, 116685. https://doi.org/10.1016/j.jsv.2021.116685

[44] Jeon, W., Son, T., Park, S., 2024. Lightweight waveguide absorbers based on spiral acoustic black holes for reducing structural vibrations in mechanical systems. *INTER-NOISE and NOISE-CON Congress Proceedings*, 25-29 August, Nantes, France, 10013-10016. https://doi.org/10.3397/IN_2024_4344

[45] Zhang, Y., Tong, M., Huang, K., Yang, F., Rui, X., 2024. Experimental investigation into the acoustic black hole vibrating absorbing effect and its automotive application. *Proceedings of the 2nd International Conference on Mechanical System Dynamics*, 1-5 September, Beijing, China, 1077-1086. https://doi.org/10.1007/978-981-99-8048-2_70

[46] Ungar, E.E., Kurzwell, L.G., 1984. Preliminary evaluation of waveguide absorbers. *Technical Report ADA140743*. https://doi.org/10.21236/ADA140743

[47] Lee, G.G., 1988. Analytical and experimental studies of beam waveguide absorbers for structural damping. *Technical Report ADA195085*.

[48] Watson, S.J., 1989. Experimental studies of circular viscoelastic waveguide absorbers for passive structural damping. *Master Thesis*, Naval Postgraduate School, Monterey, California, USA.

[49] Bowyer, E.P., Krylov, V.V., 2014. Damping of flexural vibrations in turbofan blades using the acoustic black hole effect. *Applied Acoustics*, 76, 359-365. https://doi.org/10.1016/j.apacoust.2013.09.009

[50] Deng, J., Guasch, O., Maxit, L., Zheng, L., 2020. Reduction of Bloch–Floquet bending waves via annular acoustic black holes in periodically supported cylindrical shell structures. *Applied Acoustics*, 169, 107424. https://doi.org/10.1016/j.apacoust.2020.107424

[51] Liu, B., Zhang, H., Wang, K., Wu, J., 2019. Acoustic black hole lightweight superstructure with low-frequency broadband high-efficiency sound insulation mechanism and experimental study. *Journal of Xi'an Jiaotong University*, 53, 128-134.

[52] Kyaw Oo D'Amore, G., Rognoni, G., Biot, M., Mauro, F. 2023. Acoustic black holes: The new frontier for soundproofing on board ships. *Advances in the Analysis and Design of Marine Structures*. https://doi.org/10.1201/9781003399759-20

[53] Jiao, J., Chen, Z., Xu, S. 2024. CFD-FEM simulation of water entry of aluminium flat stiffened plate structure considering the effects of hydroelasticity. *Brodogradnja*, 75(1), 75108. https://doi.org/10.21278/brod75108

[54] Krylov, V.V., Tilman, F.J.B.S., 2004. Acoustic black holes for flexural waves as effective vibration dampers. *Journal of Sound and Vibration*, 274, 605-619. https://doi.org/10.1016/j.jsv.2003.05.010

[55] Krylov, V.V., Winward, R.E.T.B., 2007. Experimental investigation of the acoustic black hole effect for flexural waves in tapered plates. *Journal of Sound and Vibration*, 300, 43-49. https://doi.org/10.1016/j.jsv.2006.07.035

[56] Deng, J., Ling, Z., Zeng, P., Zuo, Y., Guasch, O., 2018. Passive constrained viscoelastic layers to improve the efficiency of truncated acoustic black holes in beams. *Mechanical Systems and Signal Processing*, 118, 461-476. https://doi.org/10.1016/j.ymssp.2018.08.053

[57] Kim, S., Lee, D., 2018. Numerical analysis of wave energy dissipation by damping treatments in a plate with acoustic black holes. *Journal of Mechanical Science and Technology*, 32, 3547-3555. https://doi.org/10.1007/s12206-018-0705-8

[58] Aklouche, O., Pelat, A., Maugeais, S., Gautier, F., 2016. Scattering of flexural waves by a pit of quadratic profile inserted in an infinite thin plate. *Journal of Sound and Vibration*, 375, 38-52. https://doi.org/10.1016/j.jsv.2016.04.034

[59] Lee, J.Y., Jeon, W., 2019. Exact solution of Euler–Bernoulli equation for acoustic black holes via generalized hypergeometric differential equation. *Journal of Sound and Vibration*, 452, 191-204. https://doi.org/10.1016/j.jsv.2019.02.016

[60] Hobby Metals and Plastics, 2024. Plastica Delrin POM-C. https://hmpsrl.it/categoria-prodotto/plastica/delrin-pom-c/ (accessed 9th September 2025)

[61] O'Boy, D., Krylov, V. V., Kralovic, V., 2010. Damping of flexural vibrations in rectangular plates using the acoustic black hole effect. *Journal of Sound and Vibration*, 329 (22), 4672-4688. https://doi.org/10.1016/j.jsv.2010.05.019

[62] Georgiev,V. B., Cuenca, J., Gautier, F., Simon, L., Krylov, V. V., 2011. Damping of structural vibrations in beams and elliptical plates using the acoustic black hole effect. *Journal of Sound and Vibration*, 330, 2497-2508. https://doi.org/10.1016/j.jsv.2010.12.001

[63] Rognoni, G., D'Amore, G., Brocco, E., Biot, M. 2022. Improvements in the Characterization of Viscoelastic Materials for Marine Applications. *Proceedings of 26th International Scientific Conference Transport Means 2022*, 5-7 October, Kaunas, Lithuania.

[64] Spalding, A.B., Mann, J.A., 1995. Placing small constrained layer damping patches on a plate to attain global or local velocity changes. *Journal of the Acoustical Society of America*, 97, 3617-3624. https://doi.org/10.1121/1.412444

[65] Kruger, D. H., Mann, J. A., Wiegandt, T. 1997. Placing constrained layer damping patches using reactive shearing structural intensity measurements. *Journal of Acoustic Society of America*, 101, 2075-2082. https://doi.org/10.1121/1.418243

[66] Baz, A.M., 2019. Active and passive vibration damping. *John Wiley & Sons*. https://doi.org/10.1002/9781118537619

[67] Pavić, G., 1976. Measurement of structure-borne wave intensity, Part I: Formulation of the methods. *Journal of Sound and Vibration*, 49(2), 221-230. https://doi.org/10.1016/0022-460X(76)90498-3

[68] Gavrić, L., Pavić, G., 1993. A finite element method for computation of structural intensity by the normal mode approach. *Journal of Sound and Vibration*, 164, 29-43. https://doi.org/10.1006/jsvi.1993.1194

[69] Alfredsson, K.S., Josefson, B.L., Wilson, M.A., 1996. Use of the energy flow concept in vibration design. *AIAA Journal*, 34(6), 1250-1255. https://doi.org/10.2514/3.13220

[70] Alfredsson, K.S., 1997. Active and reactive structural energy flow. *Journal of Vibration and Acoustics*, 119(1), 70-79. https://doi.org/10.1115/1.2889689

[71] Gavrić, L., Pavić, G., Carinel, X., 1990. Structure-borne intensity fields in plates, beams and plate–beam assemblies. *Proceedings of the 3rd International Congress on Intensity Techniques*.

[72] Rognoni. G., D'Amore G., Brocco, E., Moro, L., Biot, M. 2023. Investigation on the Impact of a Metamaterial Solution for the Mitigation of Noise Radiated by a Ship Panel. *Proceedings of the 33rd International Ocean and Polar Engineering Conference. International Society of Offshore and Polar Engineers (ISOPE)*, 18-23 June, Ottawa, Canada.

[73] Pavić. G. 2005. The role of damping on energy and power in vibrating systems. *Journal of Sound and Vibration*, 281, 45-71. https://doi.org/10.1016/j.jsv.2004.01.030

[74] Nilsson, A., Liu, B., 2015. Vibro-acoustics, Volume 1. *Springer*, Berlin. https://doi.org/10.1007/978-3-662-47807-3